Plasma Sources
Science and
Technology

Foundations of plasma-assisted combustion. Part 2. Mechanisms and applications.

Foundations of plasma-assisted combustion. Part 2. Mechanisms and applications.

C O Laux[1], J-B Perrin-Terrin[1], V Lafaurie[2], S M Starikovskaia[2].

[1] Université Paris-Saclay, CNRS, CentraleSupélec, Laboratoire EM2C, 91190 Gif-sur-Yvette, France
[2] Laboratoire de Physique des Plasmas (LPP), CNRS, Observatoire de Paris, Sorbonne Université, Université Paris-Saclay, École polytechnique, Institut Polytechnique de Paris, 91120 Palaiseau, France

christophe.laux@centralesupelec.fr, svetlana.starikovskaia@lpp.polytechnique.fr

Abstract

In Part 1 of this Foundation paper, we introduced the main concepts and the basic principles of combustion and plasmas. Part 2 will now examine the topic of Plasma-Assisted Combustion (PAC) with an emphasis on applications to novel combustion systems, particularly those of importance for energy transition. We start by providing an overview of laboratory experiments that have helped unveil the main fundamental mechanisms of PAC. We also describe some of the main advances achieved in numerical simulations of these rich and complex phenomena in three dimensional, turbulent flames. We then review applications of PAC to practical combustion systems representative of industrial configurations, emphasizing flame stabilization, lean blow-off limit extension, thermo-acoustic instability control, supersonic combustion and plasma detonation engines. Special attention is paid to the reduction of pollutants and the optimization of plasma power.

Contents

1 Challenges in combustion applications

Future combustion systems face many challenges, foremost meeting low CO_2 and pollutant emissions for a wide range of operating conditions. Additionally, to reduce CO_2 emissions it is planned to substitute fossil fuels with CO_2-free fuels (hydrogen, ammonia) or CO_2-neutral fuels such as biofuels or synthetic fuels (also called e-fuels), which requires increasing fuel flexibility in the combustion chambers. To reduce pollutants, including NO_x, SO_x, particulates, and soot in hydrocarbon-air flames, the current trend in the transportation, electric power generation, and heating industries is to burn fuel in the lean premixed regime [1, 2]. This is particularly important for NO_x emissions, because NO_x production via the well-known Zeldovich reactions increases with the flame temperature. NO_x emissions can be decreased by operating in the lean combustion regime, *i.e.* with a higher air/fuel ratio than under stoichiometric conditions. However, lean-premixed combustion faces many challenges, such as the need to increase combustor operability (i.e. the ability to extend the limits of lean blow-off to prevent extinction during fast transient regimes), control thermo-acoustic instabilities, and reduce CO and unburnt fuel near blow-off [3,4]. For the aviation sector, other challenges include the ability to relight aircraft engines under the cold and low-pressure conditions encountered at high altitudes. For supersonic engines, the objective is to enhance ignition and mixing to ensure efficient combustion.

The combustion of CO_2-neutral fuels faces the same challenges as those of fossil fuels. In addition, it is necessary to address the fuel flexibility challenges associated with the variability in combustion properties of the different types of CO_2-neutral fuels. For CO_2-free fuels, the control of NO_x emissions poses different challenges for hydrogen-air flames and NH_3-air flames. Under stoichiometric conditions, hydrogen-air flames reach higher temperatures than hydrocarbon-air flames, and therefore it is even more important to operate under lean conditions to reduce NO_x emissions. For ammonia-air flames, in contrast, NO_x emissions peak in the lean regime, as a result of fuel-bound reactions (*i.e.* reactions corresponding to the production of nitrogen atoms by dissociation of the fuel). Thus, different strategies must be used for ammonia-air flames.

Plasma-Assisted Combustion (PAC) has emerged as an innovative solution to address these challenges, thus helping reach the full potential of novel combustion systems. Several types of discharges, including Dielectric Barrier Discharges (DBD), Direct Current (DC) discharges, gliding arcs, microwave discharges, and Nanosecond Repetitively Pulsed (NRP) discharges, have been used to generate plasmas for PAC applications, as described in several review papers [5, 6]. Lean-flame stabilization, key in NO_x emission reduction, lean blow-off limit extension, and thermo-acoustic instability control, has been less documented than ignition enhancement in previous reviews ([5–8]). It is therefore one of the main topics of this article. Plasma-assisted stabilization of lean flames requires plasma sources that can be applied continuously over extended periods of time with a power much lower than the thermal power of the flames. For these reasons, NRP discharges (introduced at Stanford University [9]), gliding arcs, and DBD discharges have been widely used for such applications.

The following sections provide an overview of current progress in PAC from fundamental understanding to industrial applications. Although the main focus is placed on hydrocarbon fuels owing to the much larger body of literature available for these traditional fuels, a few recent advances on plasma-assisted combustion of hydrogen and ammonia flames will also be mentioned. Section 2 begins by exploring the ability of plasma to extend the lean blow-off (LBO) limits of combustors in academic configurations. It then describes the fundamental thermo-chemical mechanisms of flame stabilization by nonequilibrium plasmas. Following this, the state-of-the-art in numerical simulations of complex, three-dimensional, turbulent, plasma-assisted flames is reviewed. The section concludes with a study of LBO extension in a model combustor representative of the next generation of staged aeronautical engines. Section 3 focuses on the impact of discharges on flame dynamics and thermo-acoustic instabilities (TAI), reviewing several experiments to mitigate and control TAI using plasma. The underlying physical mechanisms are also discussed, along with an example of flame stabilization in a staged combustor representative of gas turbines for electric power generation. Section 4 addresses the mechanisms of pollutant formation, particularly NO_x and CO, in plasma-assisted flames. Finally, section 5 explores the application of plasma-assisted combustion to supersonic combustors and pulse detonation engines (PDE).

2 Extension of operability limits: lean blow-off

The capability to sustain ultra-lean combustion is important for turbine manufacturers as it increases the operability range of the systems. For example, in a gas turbine, the fuel flow rate is controlled by an injection pump and the air flow rate by the rotation of the compressor. When the thermal power needs to be reduced, the fuel injection is decreased. The equivalence ratio immediately drops as the air flow rate is kept constant because of the inertia of the rotor. Therefore, the power decrease rate is controlled by the LBO limit. Extending the LBO limit allows faster power transitions.

2.1 Lean blow-off experiments in lab-scale combustors

Lean-flame stabilization by nonequilibrium plasmas was successfully demonstrated in several experiments with laboratory-scale combustors. Most of these experiments used NRP discharges, with voltage pulses of nanosecond duration (typically 10 ns), high amplitude (typically 10 kV), applied at frequencies of 10-300 kHz [10–22]. Information about the nomenclature used to describe the various types of NRP discharges is provided in the appendix. A few experiments were also performed with DBD discharges [23], microwave discharges [24], or gliding arcs [25–28].

Figure 1 illustrates a demonstration by Di Sabatino *et al.* of lean blow-off extension using NRP discharges [16]. The experiment was conducted on a bluff-body swirled stabilized burner operated with premixed air and CH_4. For pressures from 1 to 5 bars, the flame becomes unstable when the equivalence ratio decreases. Applying the NRP discharges allows the flame to anchor back to the bluff-body and thus the operability range increases.

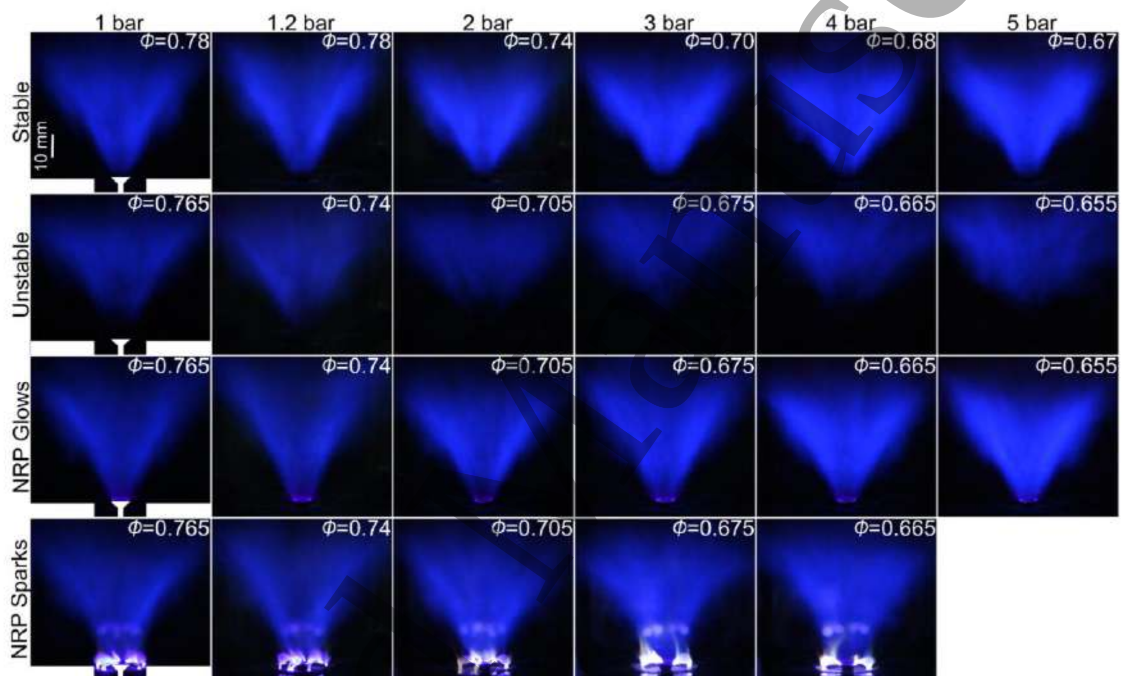

Figure 1: Stabilization of a lean swirled methane-air flame in the H-PPAC test rig, at pressures between 1 and 5 bars. NRP discharges are switched on in lines 3 and 4. Reproduced from DiSabatino *et al.* [16].

Table 1 summarizes the operating conditions of several illustrative experiments from the literature. The last column indicates by how much the LBO limit was extended with plasma *vs.* without plasma. These experiments were conducted with a variety of configurations, including laminar, bluff-body, swirled, and staged burners.

Laminar burners are used for fundamental studies to measure laminar flame properties, important in modeling and theory. Bluff-body and swirled burners are used to stabilize flames when the flow velocity is higher than the flame speed by creating a recirculation region where the flame can anchor.

In bluff-body burners, the recirculation zone is created by an obstacle (the bluff body) placed in the high-speed flow. These burners are typically used for fundamental research and industrial furnaces.

In swirled burners, the recirculation zone is created by injecting the flow (or part of it) with a strong tangential velocity. This creates a vortex with a depression at its center causing the flow to recirculate (see figure 11 about vortex breakdown mechanisms). Compared to bluff-body burners, swirled burners provide more compact flames and better stabilization in high-speed flows. They are widely used for power gas turbines and jet engines.

In staged burners, the injection of fuel and/or air is divided into several stages to reduce NO_x emissions by optimizing fuel/air mixing (see Section 2.3). Staged burners are used in advanced industrial gas turbines and jet engines. Two academic examples will be discussed in Sections 2.3 and 3.4. The LDI (Lean Direct Injection) burner is another advanced strategy to achieve ultralow NO_x emissions, in particular for aerospace propulsion [29].

In the various experiments reported in Table 1, the LBO was extended by 5% to 75% depending on the type of burner, fuel, pressure, and plasma parameters. Several important conclusions can be drawn from these experiments:

- Nonequilibrium plasmas can stabilize lean flames with a wide variety of fuels, including gaseous hydrocarbon fuels (natural gas, methane, propane), liquid hydrocarbons (kerosene, synthetic fuels such as heptane and dodecane), as well as zero-carbon fuels (hydrogen, ammonia).
- The electric power consumption of the plasma is very low, typically less than 0.1–1% of the flame thermal power.
- NRP discharges have been shown to work effectively up to at least 5 bars. This is promising for industrial applications but additional studies are needed at the significantly higher operating pressures (∼30 bars) of real combustors.

- Electrode configurations vary with burner geometry and constraints, and are often integrated into the injection system —- for example, bluff bodies commonly serve as electrodes. At atmospheric pressure, typical gap distances are around 5 mm. An optimal configuration has yet to be identified.

- There is a wide variety of electrode configurations and the optimal setup depends on the geometry and constraints of each burner. In general, typical interelectrode gaps are ∼5 mm for the experiments at atmospheric pressure.

Although gliding arcs have not been investigated for a wide range of conditions, they seem to offer similar performances as NRP discharges for plasma-assisted flame stabilization. They may become interesting for combustion stabilization at high power, since they can typically deliver a higher average power than NRP discharges. On the other hand, NRP discharges enable a more precise control of the deposited plasma energy.

Table 1: Experiments on lean flame stabilization with various types of discharges. The last column indicates the degree of extension of the lean stability or LBO limit: the fuel equivalence ratios without and with plasma are indicated when only one condition was investigated, otherwise we indicate the average percentage of decrease of fuel equivalence ratio. The swirled-staged stabilized combustor experiments of Blanchard 2023 [19, 30] are further discussed in section 2.3

Reference	**Burner type Electrode setup – gap distance**	**Fuel**	**P (bar)**	**Flame power (P_{flame})**	**Plasma power (P_{plasma})**	$\frac{P_{plasma}}{P_{flame}}$	**f_{rep} (kHz)**	**LBO or stability extension**
				NRP Discharges				
Pilla 2006 [10]	Bluff-body Pin/Pin – 5 mm	Propane	1	11 kW	70 W	0.6%	30	$\sim$ 10%
Heid 2009 [15]	Swirled Pin/Ring – $\sim$ 3 mm	Kerosene	3	50 kW	< 500 W	< 1%	30	0.44 → 0.21
Kim 2010 [11]	Swirled Mesoscale Array Pin/Pin – 1 mm	Methane	1	–	10 W	–	15–50	$\sim$ 10%
Pham 2011 [12]	Bluff-body Pin/Pin – 5 mm	Methane	1	11 kW	70 W	0.6%	30	$\sim$ 10%
Barbosa 2015 [13]	Swirled staged Pin/Ring – $\sim$ 10 mm	Propane	1	11 kW	350 W	3.2%	30	0.4 → 0.11
Gomez 2017 [14]	Lean Direct Injection Pin/Ring – 5 mm	Methane	3.3	50 kW	500 W	1%	30	0.21 → 0.16
DiSabatino 2020 [16]	Swirled Bluff-body Rod/Ring – $\sim$6 mm	Methane	1	4.5 kW	31 W	0.7%	30	$\sim$ 5%
DiSabatino 2020 [16]	Swirled Bluff-body Rod/Ring – $\sim$6 mm	Methane	5	20 kW	65 W	0.3%	30	$\sim$ 5%
Vignat 2021 [17]	Swirled Spray Pin/Plane – 5 mm	Methane, Heptane, Dodecane	1	5 kW	< 100 W	< 2%	20	$\sim$ 10%
Choe 2021 [18]	Swirled Bluff-body Rod/Ring – 7 mm	Ammonia	1	2 kW	39 W	1.9%	4	0.67 → 0.45
Blanchard 2023 [30]	Swirled staged Pin/Ring – 7 mm	Methane	1	150 kW	370 W	0.25%	100	0.56 → 0.42
Blanchard 2023 [19]	Swirled staged Pin/Ring – 7 mm	Methane	1	20–100 kW	–	< 0.5%	33	$\sim$ 40%, see fig. 9
Aravind 2023 [20]	Swirled Bluff-body Rod/Ring – 4 mm	NH_3/CH_4	1–4	7–25 kW	45–150 W	$\sim$ 0.6%	30	6–12%
Perrin-Terrin 2024 [21]	Swirled Cross-flow Pin/Pin – 2.3 mm	Hydrogen	1	2.2 kW	22 W	1%	15	0.22 → 0.18
				Dielectric Barrier Discharges				
Kim 2020 [23]	Swirled Bluff-body Rod/Ring – 4 mm	Methane	1	1–2 kW	20 W	1–2%	4	$\sim$15%
				Microwave discharges				
Michael 2013 [24]	Flat-flame Hencken NA – NA	Methane	1	750 W	75 W	10%	1	0.63 → 0.3
				Gliding Arcs				
Lin 2019 [31]	Swirled Bluff-body Rod/Cone – NA	Kerosene 5°C, -30°C	1	$\sim$ 2-10 kW	300–460 W	5–15%	$\sim$ 2	$\sim$ 40%
Tang 2021 [27]	Swirled Bluff-body Rod/Ring – 5.5 mm	Methane	1	1.3–6.6 kW	60 W	1%	7 & 25	$\sim$ 40%
Liu 2022 [26]	Swirled staged – Rod/Cone – NA	Methane	1	78 kW	8 W	0.1%	5	0.47 → 0.45

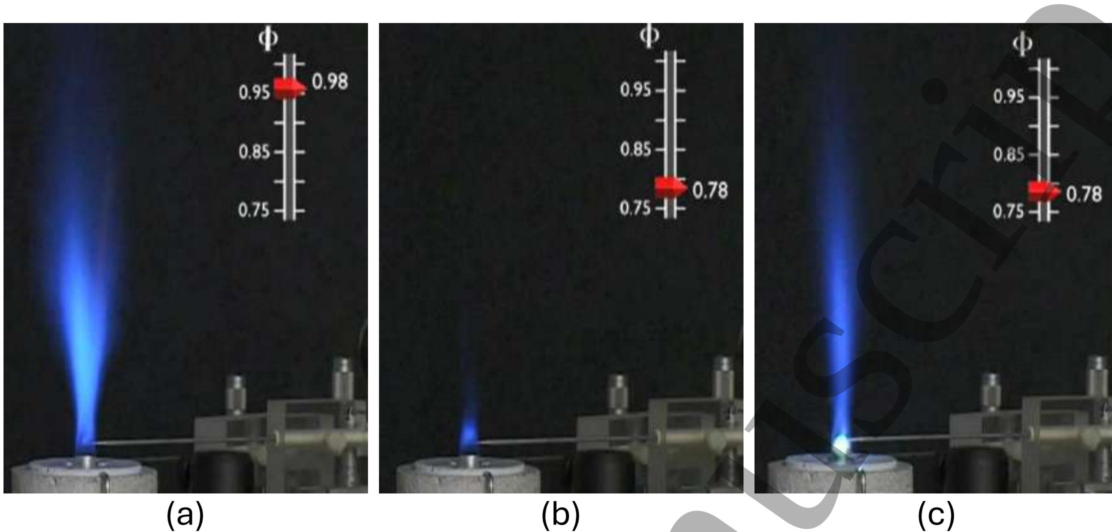

Figure 2: Stabilization of a propane-air flame at 1 bar (Mini-PAC burner) with NRP discharges. (a) Stable stoichiometric flame ($\phi \approx 1$) without plasma. (b) Lean flame ($\phi \approx 0.78$) near LBO limit, without plasma. (c) Lean flame ($\phi \approx 0.78$) stabilized by NRP discharge. The electric power of the NRP discharge is 75 W, which is 0.7% of the 11 kW thermal power of the flame [10]. In these experiments, the transition from stoichiometric to lean flame is obtained by increasing the air flow rate while keeping the propane flow rate constant.

2.2 Mechanisms of flame stabilization

2.2.1 Experimental observations

Figure 2 shows a lean propane-air flame stabilized by an NRP discharge (2.5 mJ/pulse, 30 kHz pulse repetition frequency). This experiment was conducted in the Mini-PAC facility, a 15-kW laboratory-scale combustor at atmospheric pressure operated at the EM2C laboratory [10]. The premixed flame is stabilized by a bluff body, as described in figure 3. Premixing is obtained by counter-injecting propane and air at the bottom of the tube. Without plasma, the flame extinguishes at a fuel equivalence ratio $\phi = 0.78$ for the conditions of figure 2. When NRP discharges are applied at the base of the flame, a stable flame is recovered.

During each voltage pulse, the gas located in the interelectrode region is excited, dissociated, and ionized via electron-impact reactions as detailed in section 3.2 of the companion article [32]. In air-fuel mixtures, most of the discharge energy is spent to excite various electronic states of N_2, in particular $A^3\Sigma_u^+$, $B^3\Pi_g$, $a'^1\Sigma_u^-$, $C^3\Pi_u$,

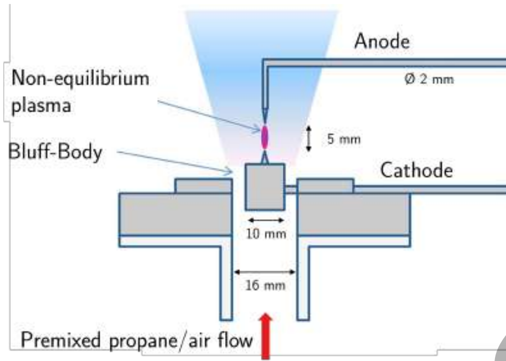

Figure 3: Schematic of the mini-PAC burner, adapted from Pilla *et al.* [10].

collectively noted N_2*. The remaining energy of the discharge excites other species (in particular the vibrational states of N_2), which subsequently decay via processes such as vibrational-translational relaxation, resulting in slow gas heating on time scales on the order of 10-100 µs. Immediately after the end of the pulse, N_2* reacts with the species present in the gap (O_2 and fuel, as well as CO_2 and H_2O since the discharge is located in the burnt gases). Reactions of N_2* with molecular species lead to dissociative quenching, such as in the following examples:

$$N_2^* + O_2 \rightarrow N_2 + O + O + \Delta T \tag{1}$$

$$N_2^* + CO_2 \rightarrow N_2 + CO + O + \Delta T \tag{2}$$

The dissociative quenching reactions have typical characteristic time scales on the order of 10 ns. This is known as the *ultrafast mechanism of dissociation and gas heating*, first proposed by Popov [33] and experimentally demonstrated in [34–39]. This ultrafast mechanism dissociates nearly all O_2 molecules present in the gap and increases the temperature by about 1000 K within a few tens of nanoseconds following the pulse. The produced O radicals then quickly react with fuel molecules, noted RH, resulting in the production of the free radicals OH and R. The typical time scale for OH radical production is about 10 µs. If the discharge is produced in the fresh gases, these radicals can initiate the chain propagation reactions of combustion. If the discharge is produced in the burnt gases, long-lived radicals such as OH (lifetime on the order of ms) are transported toward regions with fresh fuel, where they initiate combustion reactions. The latter process is illustrated below with the case of the Mini-PAC flame.

Xu *et al.* [40, 41] studied the transition from the unstable flame of figure 2b to the NRP-stabilized flame of figure 2c with pulses of 7 kV amplitude, 10 ns duration, and

30 kHz frequency. To elucidate the stabilization mechanism, they performed synchronized measurements of OH with Planar Laser-Induced Fluorescence (PLIF) and of CH* chemiluminescence in the recirculation zone behind the bluff-body. Figure 4 shows temporally resolved composite images of the OH and CH* concentration fields induced by the plasma. The O atoms produced by ultrafast dissociation between the electrodes quickly oxidize the fuel to form OH radicals. These OH radicals are then convected within the recirculation region and, after about 3 ms, reach the edge of the shear layer between the fresh gases and the recirculation zone. At about 4 ms, CH* appears at the bottom of the shear layer, indicating ignition of the fresh gases. The flame then develops in the shear layer region. Stabilization is achieved after about 10 ms, which corresponds to the characteristic time of flow recirculation behind the bluff-body.

2.2.2 Stabilization mechanism and characteristic time scales

The mechanism of flame stabilization is summarized schematically in figure 5. The long-lived radicals and heat produced by each pulse are convected within the recirculation region behind the bluff body. They are transported toward the edges of the burner and ignite the fresh gases when they reach the shear layer. There are several time scales of interest in this process: the residence time of the gas within the interelectrode gap, τ_{res}, the characteristic recirculation time behind the bluff body, τ_{recirc}, and the period between two pulses, $T_{\mathrm{pulse}} = 1/f_{\mathrm{rep}}$. To generate radicals, the gas must experience at least one pulse when it traverses the interelectrode gap. Thus, the residence time of the gas between the electrodes must be longer than the time between two pulses. For typical gas velocities on the order of 5 m/s and gap distances of 5 mm, pulse repetition frequencies (PRF) should be approximately 10 kHz or higher. This is an important criterion for the design of stabilization or ignition in PAC. The characteristic recirculation time behind the bluff body is also important because it determines the characteristic response time of the flame to the plasma.

2.2.3 Numerical simulations and experimental validation

Simulating plasma-assisted turbulent flames is a complex multi-physics problem involving plasma chemistry, combustion chemistry, turbulence, and heat transfer. As mentioned in section 2 of the companion article [32], these phenomena occur over a wide range of time ($10^{-9} - 1$ s) and length scales ($10^{-6} - 1$ m). Several detailed kinetic mechanisms for plasma-assisted combustion have been developed over the years [6, 43–51], and 1-D or 2-D simulations of PAC with hydrogen and low-order hydrocarbons in simple laminar and quiescent cases have been performed. For ex-

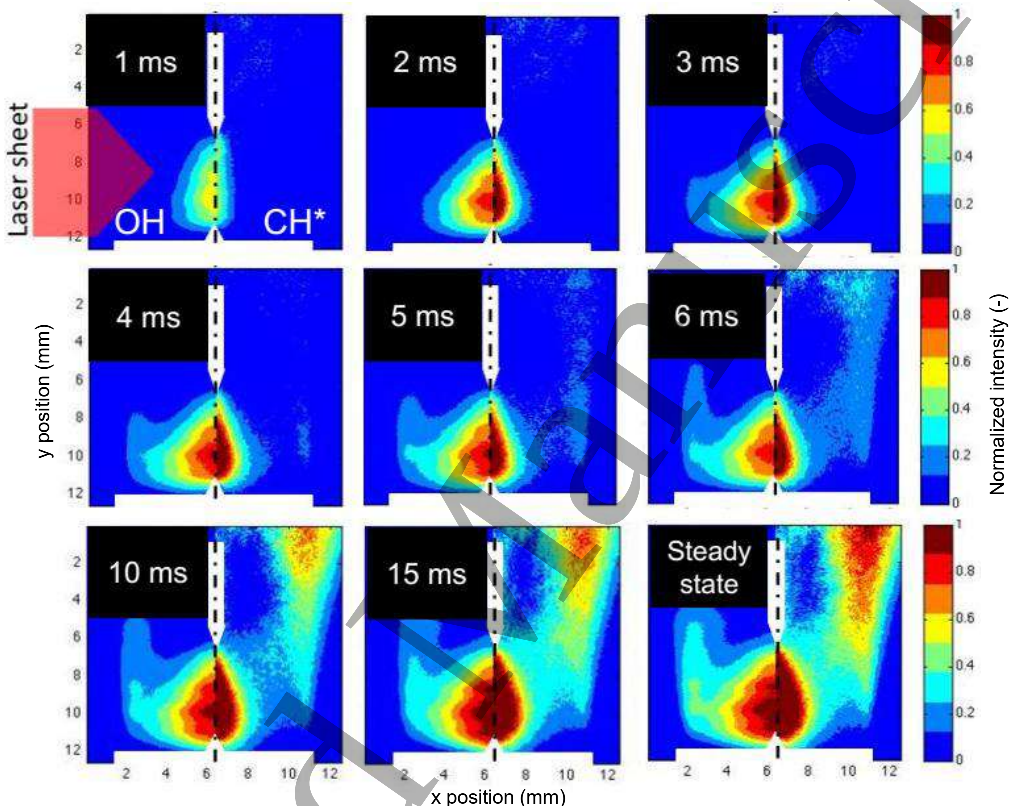

Figure 4: Composite images showing (left) normalized OH-PLIF images and (right) normalized CH* emission images in the bluff-body region during the sequence of stabilization of a lean propane-air Mini-PAC flame by a series of nanosecond pulses at 30 kHz [40,41]. The CH* emission of the flame without plasma is subtracted from the images. Adapted from Xu *et al.* [40]; reprinted by permission of the American Institute of Aeronautics and Astronautics, Inc.

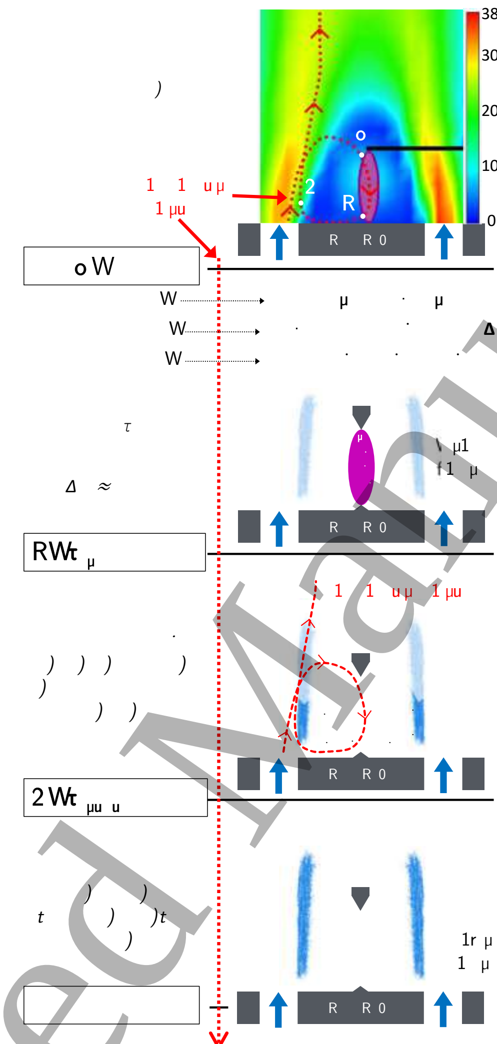

Figure 5: Mechanism of flame stabilization in a bluff-body configuration following a gas particle trajectory (top: Planar Laser-Induced Velocimetry image reproduced from Pilla [42]). The stabilization mechanism proceeds in three steps. Step 1 between A and B: generation of active species and heat by the discharge pulse. The gas experiences N_{pulses} during its residence time τ_{res} between the electrodes. Step 2 between B and C: transport of active species and heat toward the shear layers. Step 3 after C: stabilization of flame front.

ample, Bak *et al.* [52] simulated PAC in a laminar premixed methane/air 2D flame; Yin *et al.* [53], Tholin *et al.* [54], and Sharma *et al.* [55] simulated the ignition of quiescent H_2/air mixtures in 2D; Pavan and Guerra-Garcia [56] modeled the two-way interactions in 1D between a plasma and a flame. However, 3D simulations in turbulent conditions with detailed plasma and combustion chemistry are not feasible today because of their high computational cost, especially given the wide range of spatial scales required to model a combustion chamber. Even with reduced plasma-induced kinetic mechanisms [48, 49], the computational cost of solving the coupled problem with the Poisson equation, the Boltzmann equation for electrons, the continuity equation for the various species, and the Navier-Stokes equations remains prohibitive.

To answer this challenge, Castela *et al.* [57] introduced a phenomenological model to simulate the main plasma effects in air, namely ultrafast heating and O_2 dissociation, thus removing the stringent requirements of solving detailed plasma chemistry. The assumptions of the model are based on theoretical and experimental observations described in section 3.2 of the companion article [32]. For any air/fuel mixture, the model assumes that 55% of the discharge energy is spent on ultrafast processes (20% heating and 35% O_2 dissociation) lasting a few tens of nanoseconds, and the remaining 45% on vibrational excitation of N_2, which then relaxes at millisecond time scales and slowly transfers heat to the gas over a few tens of microseconds. As discussed later, this breakdown has provided quantitative simulations in agreement with PAC experiments in lean methane-air and hydrogen-air flames. Although the model remains to be tested with other fuels, it is expected that the breakdown will not vary much because a significant part of the ultrafast heating and dissociation are due to the excess oxygen molecules present in lean flames. If there is less O_2 in the mixture, the fraction of energy spent on ultrafast processes decreases proportionally, and the fraction of vibrational excitation of N_2 increases. The originality of this model is to capture both ultrafast and slow plasma phenomena. Because only one balance equation for the vibrational energy is added to the standard reactive flow balance equations, the increase of the computational cost is very limited. Thhus, the model of Castela *et al.* is a good starting point to simulate PAC in any fuel, including complex fuels for which detailed PAC mechanisms are not available.

The model of Castela *et al.* [57] was used by Bechane and Fiorina [58] and Blanchard *et al.* [59] to perform 3D simulations of plasma-assisted flames. These simulations were conducted with LES (Large Eddy Simulations), a widely used method in turbulent combustion modeling [60].

Blanchard *et al.* [59] experimentally validated the model of Castela *et al.* [57] for the stabilization of a turbulent methane-air flame in the Mini-PAC burner. In that work, quantitative measurements of temperature and OH radical concentrations were performed during a sequence of pulses leading from the nearly extinguished flame (figure 2b) to the plasma-stabilized flame (figure 2c), and compared with the results of LES. A selected set of comparisons are shown in figure 6. More details are given in [59]. As seen in figure 6a, the flame stabilizes in about 5 ms (100 pulses), a time comparable with the characteristic recirculation time of the flow behind the bluff body, in accordance with the observations made in section 2.2.1. In the middle of the interelectrode gap, the temporal evolution of the gas temperature measured from the rotational temperature of the second positive system of N_2 (figure 6b), and the OH spatial profiles measured with Laser Induced Fluorescence (figure 6c), are closely reproduced by LES.

In a related study, Bechane and Fiorina [58] performed LES simulations of the ignition of the Mini-PAC flame with NRP discharges. Using the model of Castela *et al.*, the flame ignited within about 10 pulses. To test the importance of chemical versus thermal effects, they also simulated a case assuming that 55% of the energy went into ultrafast heating and 45% into slow heating (*i.e.*, neglecting the nonequilibrium chemistry induced by the discharge). In that case, the flame did not ignite even after 100 pulses. This important finding shows that *the nonequilibrium chemistry induced by NRP discharges is the main mechanism for flame enhancement in PAC.*

Recently, Malé *et al.* [61] also showed that kinetic simulations of PAC in natural gas-hydrogen-air flames conducted with the model of Castela *et al.* [57] were in excellent agreement with those obtained with the PACMAN detailed kinetic model of Bellemans *et al.* [48, 49].

Based on these promising results, variants and refinements of the model of Castela *et al.* were recently proposed to incorporate the effects of additional plasma reactions [30, 62–64]. These models were successfully applied in LES to study various phenomena induced by NRP discharges such as turbulent flame ignition [58,65], LBO limit extension in staged combustors [61,62] and H_2 swirl-stabilized flames [66], NO_x formation [67], thermo-acoustic instability suppression [68, 69], NH_3-H_2-air combustion [63], and ignition kernel development [64]. These works show that phenomenological models such as those of Castela *et al.* [57] can quantitatively capture the main mechanisms of plasma-assisted combustion. Thus the modeling of NRP plasmas in flames is now well in hand and can be used to understand the effects of plasma-assisted combustion and to design and optimize practical systems.

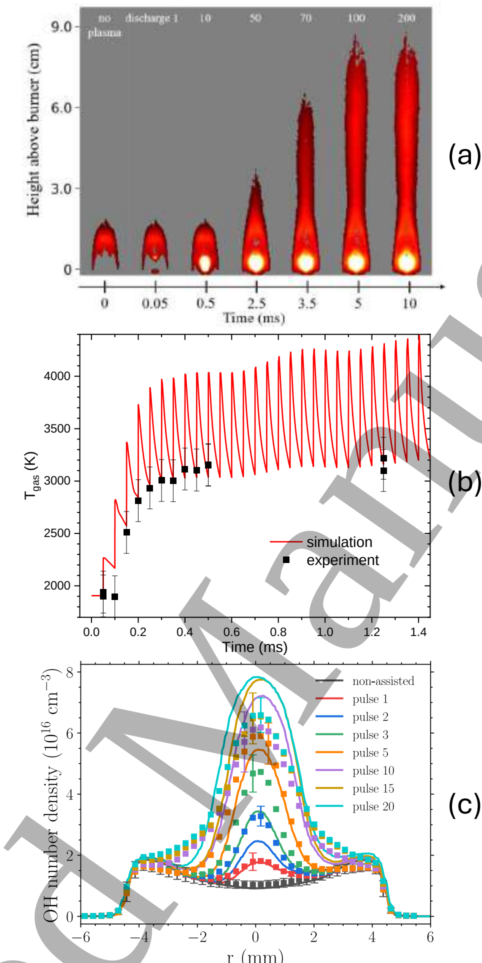

Figure 6: (a) Abel-inverted average OH* chemiluminescence images of the methane-air flame evolution under the effect of a burst of discharges with 1.8 mJ/pulse applied at 20 kHz (Mini-PAC burner). (b) Comparison of the experimental temperature evolution (black symbols) and numerical predictions (red line) in the discharge region during the stabilization sequence. (c) Comparison of the experimental radial profiles of OH density measured 45 µs after each discharge in the middle of the interelectrode gap (squares) with the profiles obtained with LES at the same time and location (solid lines) during the stabilization sequence [59].

2.3 Lean blow-off extension in a model aeronautical combustor

As previously mentioned, industry faces difficulties in reaching low emissions using conventional combustors. To illustrate this point, figure 7 shows the emissions of CO and NO_x, two of the main pollutants emitted by combustion, as a function of the temperature of the primary combustion zone. For hydrocarbon fuels, only a narrow band of temperatures allows for low emissions of both pollutants. A conventional combustor usually operates with only one type of injector. If the injector is designed for low NO_x emissions at high power, incomplete combustion, and thus increased CO emissions, will occur at lower power. To circumvent these limitations, a promising approach is to use two injectors generating two combustion zones: the first one is designed to operate in the low emission band at high power, and the second one in the low emission band at low power. This concept is called *staged combustion*. Stages can be distributed axially or radially. This concept is already used in industrial systems such as the Ansaldo GT24/GT26 gas turbine [70] or the Twin Annular Premixing Swirled (TAPS) combustor [2, 71] but still presents challenges [3].

In this section, we present a demonstration of LBO limit extension by NRP discharges in a *radially* staged injector representative of aeronautical Lean Premixed Prevaporized (LPP) injection systems [19, 72]. Experiments with an *axially* staged combustor representative of power production gas turbines will be presented in section 3.4.

The BIMER-PAC combustor of the EM2C laboratory is a radially staged combustor operating with methane and air at atmospheric pressure and with flame powers up to 150 kW. As shown in figure 8, BIMER-PAC is comprised of a plenum, an injector, and a combustion chamber with a square cross-section of 15 cm width and 50 cm length. The first stage is the pilot stage with a single injection tube of diameter 4 mm, while the second stage (multipoint stage) is an annular inlet with 15 injection holes of diameter 750 µm. Both stages create co-rotating swirled flows. A complete description of BIMER-PAC is given in [19]. The design of this injector is representative of staged LPP combustors found in aircraft engines such as the TAPS or Lean Direct Injection (LDI) combustors [2]. The pilot stage creates a fuel-rich flame used to stabilize the lean and well-premixed multipoint flame, which produces most of the power. The injection mode is characterized by a staging factor α_p, defined as the ratio of the pilot fuel over total fuel mass flow rates:

$$\alpha_p[\%] = \frac{\dot{m}_{\text{fuel, pilot}}}{\dot{m}_{\text{fuel, total}}} \tag{3}$$

The staging ratio can be adjusted with mass flow rate controllers. The air mass flow rate is distributed 80% to the multipoint stage and 20% to the pilot stage.

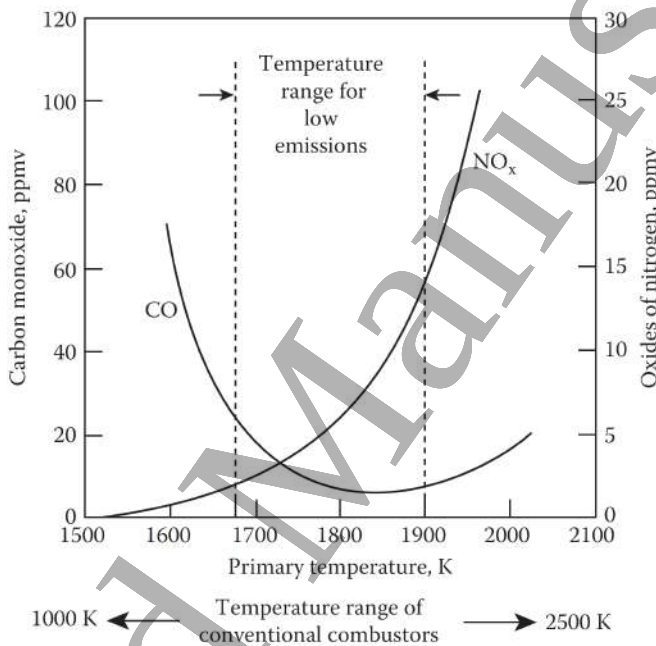

Figure 7: Influence of primary-zone temperature on CO and NO_x emissions for hydrocarbon fuels. NO_x emissions are driven by the Zeldovich mechanism. Reproduced from [1].

As shown in figure 8, NRP discharges are generated between the tip of a high voltage electrode and the outlet of the pilot stage across a 7 mm gap. The electrode crosses the flame front and is therefore exposed to high temperatures. To limit erosion, it is water-cooled. NRP discharges are applied with a voltage of 8 kV, an average energy per pulse of 3.6 mJ, and a frequency of 33 kHz [19]. This setup generates rotating spark discharges, as shown in the picture on the right of figure 8.

The effects of the NRP discharges on this injection system were first studied by Barbosa *et al.* [13], and then further investigated by Blanchard *et al.* [19] across a wider range of parameters: thermal powers between 20 and 150 kW and staging factors between 0% and 100%. Figure 9 shows the results from [19] except the 150 kW case[1]. In all conditions, the LBO limit is significantly extended with an NRP discharge power of less than 0.5% of the flame power. For $\alpha_p \geq 20\%$, the LBO limit is reduced by a factor of 2.8 in the most efficient case and 1.2 in the least efficient case, representing a significant improvement in operability for this low-NO_x combustor. To understand the mechanism of LBO extension, the authors studied the extinction sequence with CH* chemiluminescence, as shown in figure 10. Without plasma assistance, the flame follows the extinction sequence illustrated in the top row: starting as a V-shape flame, the flame intensity decreases progressively with the equivalence ratio. When the equivalence ratio is further reduced, the flame starts oscillating and quickly extinguishes. When plasma assistance is on, the flame can sustain the oscillating phase, and when the equivalence ratio decreases to 0.44, the flame takes a tulip shape and stops oscillating. The tulip flame is sustained down to an equivalence ratio of 0.38, which represents a 32% extension of the LBO limit compared with the case without plasma. The combustion efficiency of the tulip flame was measured to be around 40%, which is sufficient to sustain combustion in transient regimes, thus extending operability.

The change of flame shape is due to a change in the flow topology during the extinction sequence [73]. To understand this, it is important to note that a swirled flow presents a Central Recirculation Zone (CRZ) created by the vortex breakdown mechanism described in [74]. The CRZ is a region in the chamber where the axial velocity is negative. The flame usually stabilizes between the CRZ and the main flow because of the lower flow velocity in that region, as illustrated in figure 11. In this experiment, at high equivalence ratios, the flow presents a Conical Vortex Breakdown (CVB) mode creating a conical CRZ. The flame base anchors inside the injector and the branches follow the conical shape of the CRZ, thus shaping the flame as a V. When the equivalence ratio is decreased, the breakdown mode shifts to the Bubble

[1]The authors mentioned that at 150 kW and $\alpha_p = 40\%$ the LBO was extended from 0.56 to 0.42, but they did not repeat the experiment as the facility reached the safety limit.

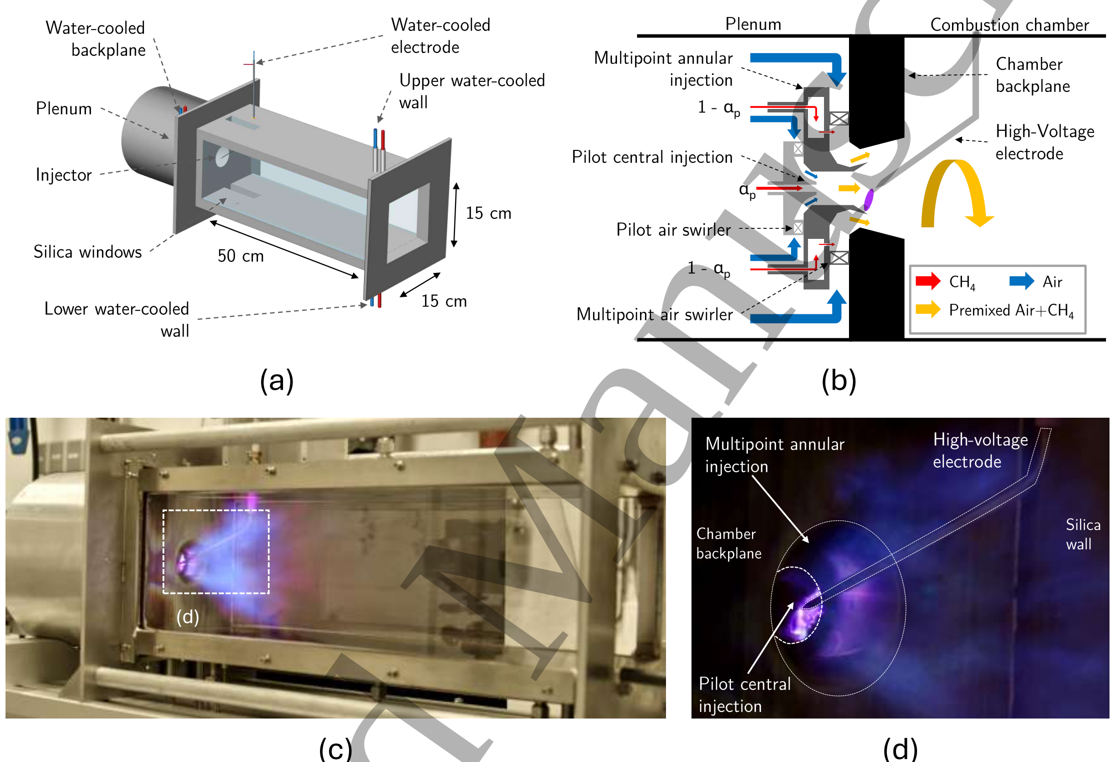

Figure 8: (a) Schematic of the BIMER-PAC combustor. (b) Schematic of the staged injector and NRP electrode system. (c) Photograph of the combustor operated at 40 kW with NRP discharges. (d) Close-up photograph of the injector with NRP discharges. Several discharges can be seen as the exposure time of the photograph is longer than the discharges repetition period.

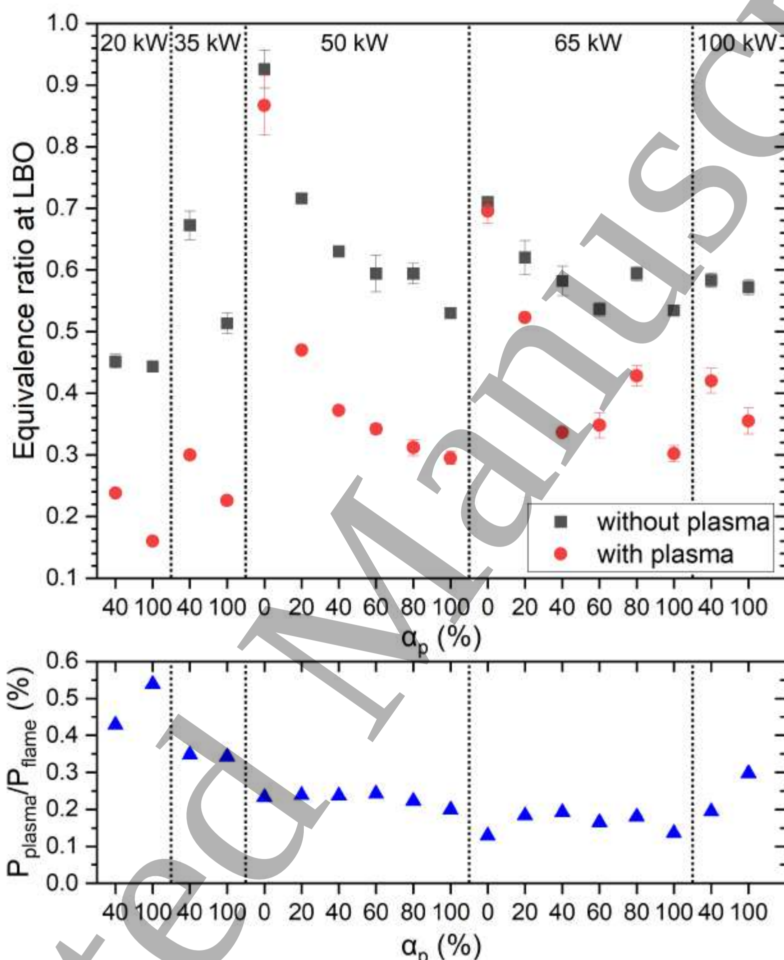

Figure 9: Top: stability map of BIMER-PAC with and without NRP discharges for different fuel staging factors (α_p is the fraction of fuel injected through the pilot stage). Bottom: plasma-to-flame power ratio. Reproduced from Blanchard *et al.* [19].

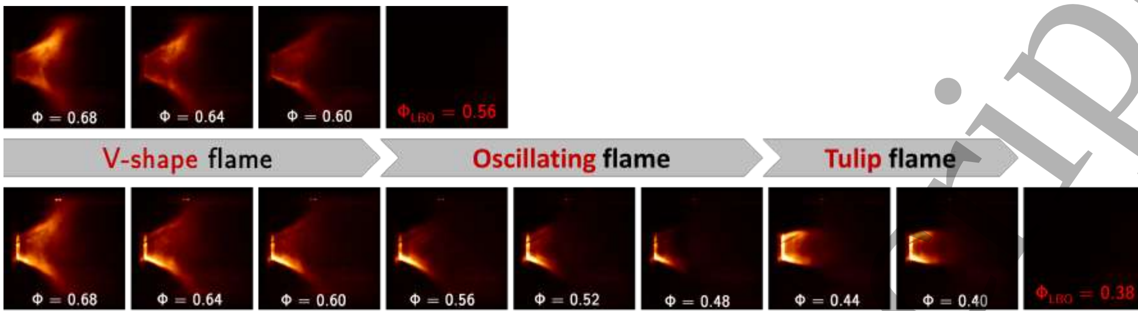

Figure 10: CH* chemiluminescence images during an LBO sequence in BIMER-PAC ($P_{\mathrm{th}} = 50$ kW; $\alpha_p = 40\%$). Top row: without discharge. Bottom row: with NRP discharges ($f_{\mathrm{rep}} = 33$ kHz, $E_p = 3.6$ mJ). [Adapted from Blanchard *et al.* [19]]. The fuel equivalence ratio is decreased by increasing the air flow rate while keeping the methane flow rate constant at 5 Nm^3/h (1 g/s).

Vortex Breakdown mode (BVB). In this mode, the CRZ forms a small central bubble, thus shaping the flame as a tulip. In the BVB mode, the mixing between the pilot stage and the multipoint flow is less effective. Therefore, the NRP discharges ignite mostly the fuel from the pilot stage, explaining the lower combustion efficiency of the tulip flame.

Finally, it should be noted that the lower performance in LBO extension at $\alpha_p = 0$ is because the plasma is created in a region with just air and no fuel. The O radicals created by the discharge recombine before being able to oxidize the fuel and form OH. Thus, no increase in performance can be achieved with the current electrode position. The authors of [19] suggested to change the electrode position to increase the performances at low staging factors.

Blanchard *et al.* [19] demonstrated that NRP discharges can improve operability of low NO_x combustors with only 0.2% of the flame power. By exploring the application of various pulse patterns instead of applying the discharges continuously at a constant repetition frequency, the plasma-to-flame power ratio required to stabilize a lean flame can be decreased to 0.06%, and pollutant emissions can be further decreased (see section 4). These results demonstrate that plasma-assisted combustion can increase the operability of real combustion systems in transient regimes, such as sudden deceleration in aircraft engines or sudden reduction of power demand in a power gas turbine.

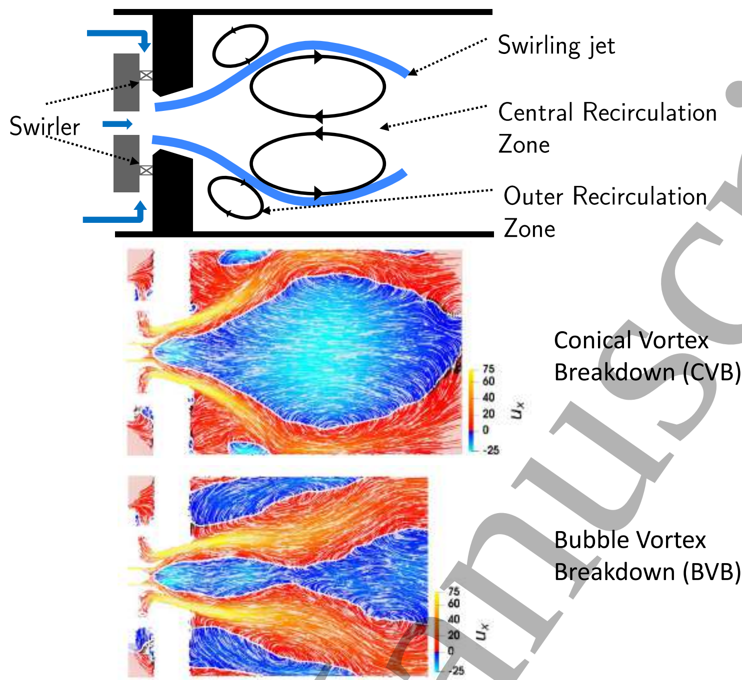

Figure 11: Simplified schematic diagram of swirled flow topology (top). Axial velocity field in a conical vortex breakdown CVB mode (middle) and bubble vortex breakdown BVB mode (bottom) as computed in [75].

3 Control of thermo-acoustic instabilities

3.1 Introduction to thermo-acoustic instabilities

Another major challenge in aero-engines and stationary gas turbines is the ability to control dynamic thermo-acoustic instabilities (TAIs). TAIs occur when the flow and the combustion fluctuations are coupled by acoustic resonant modes of the chamber as schematically shown in figure 12(a). The pressure oscillations of a TAI may reach 10% of the mean pressure and cause noise, vibrations and structural fatigue, thus potentially leading to structural damage to the chamber. They can also increase heat transfer to the combustor chamber walls and enhance pollutant emissions [4, 76, 77].

The frequencies of the oscillations depend in a complex way on the geometry of the chamber, the design of the burner, the fuel, and the operating conditions. To illustrate with a simple example, we consider the case of a combustion chamber with an open outlet. In that case, longitudinal acoustic modes occur at frequencies corresponding approximately to $nc/4L$, where n is an odd integer ($n = 1, 3, 5, \ldots$),

c is the speed of sound, and L is the length of the chamber. For an open chamber of length 1 m, taking into account the speed of sound in combustion gases to be around 800 m/s, typical frequencies of TAI oscillations are around 200 Hz (quarter-wave mode), 600 Hz (three-quarter-wave mode), and so on. The measured TAI frequencies deviate slightly from these estimated chamber mode frequencies due to a frequency shift induced by the flame dynamics [78]. The TAIs reviewed in Table 2 fall within this range of frequencies.

The development of a TAI is governed by a source term of acoustic energy, given by the Rayleigh integral, $\iiint_V p'q'\,dV$, where V stands for the volume of the flow domain, and p' and q' for the fluctuations of pressure and Heat Release Rate (HRR) per unit volume, respectively. The Rayleigh criterion [79] states that a positive Rayleigh integral is a necessary condition for the development of thermo-acoustic instabilities. As discussed in [80], to determine whether a TAI will develop, this source term must be compared to the damping term, which is the sum of the dissipation of acoustic energy in the system and the outgoing fluxes of acoustic energy. If the Rayleigh integral is lower than the damping term, the instabilities do not develop. Therefore, to mitigate TAI in engines, one can either increase the damping term or decrease the Rayleigh integral. Several methods have been proposed to mitigate TAI in engines, including passive methods such as Helmholtz dampers, and active methods with acoustic excitation using driver units or fuel flow modulation [77]. Figure 12b illustrates how active mitigation techniques can be used in a closed-loop control scheme to improve stability. However, these methods still lack flexibility, and novel actuation techniques are desirable [81]. Plasma-assisted combustion using NRP discharges offers an interesting alternative as the actuation source can be controlled by various parameters: the applied voltage, the repetition frequency, and the pulsing pattern.

To describe and predict TAIs, researchers have developed several analytical approaches [4, 78, 82, 83]. One of these tools is the Flame-Transfer Function (FTF), which characterizes the flame's response to a flow perturbation, specifically how the HRR, noted $\dot{Q}$, responds to a change in velocity, pressure, or equivalence ratio [78]. For example, for the change in velocity u, the FTF is defined as:

$$F(\omega) = \frac{\hat{\dot{Q}}(\omega)/\bar{\dot{Q}}}{\hat{u}(\omega)/\bar{u}} \tag{4}$$

where $\bar{\dot{Q}}$ is the mean value of the HRR, $\hat{\dot{Q}}$ the Fourier transform of the HRR, $\bar{u}$ the mean flow velocity, $\hat{u}$ the flow velocity Fourier transform, and ω the frequency of the perturbation. These analytical approaches help determine the safe operating range for existing systems, serve as design tools for industry and, with further development, will help understand the plasma influence on flame stabilization.

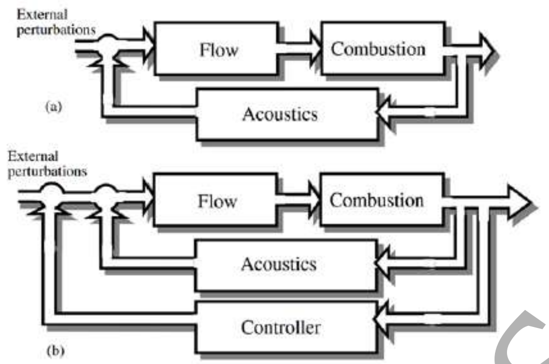

Figure 12: (a) Schematic diagram of combustion instability coupled by acoustic feedback. (b) An active control loop is used to stabilize the system. Reproduced from Candel [4].

3.2 TAI experiments in lab-scale combustors

In [84], Lacoste *et al.* showed that NRP discharges were effective in reducing Turbulence Induced Noise (TIN), *i.e.* the pressure fluctuations induced by velocity fluctuations in turbulent flames. Specifically, they showed a strong attenuation of velocity oscillations in a swirled, bluff-body stabilized methane-air flame (4 kW) at atmospheric pressure. They attributed this effect to a better anchoring of the flame close to the injector outlet thanks to the enhanced reactivity afforded by the discharges.

The control of TAI with NRP discharges was first demonstrated by Moeck *et al.* [85] in a premixed natural gas/air swirled flame at atmospheric pressure (figure 13). With the NRP discharges applied continuously at 50 kHz, the flame ($\phi = 0.66$, $P_{\text{thermal}} = 43$ kW) moved closer to the injector, and a TAI with peak pressure oscillations of 300 Pa at 150 Hz was nearly suppressed with a plasma power of 0.7% of the flame thermal power. However, they also showed that TAI instabilities (up to 2200 Pa) could be promoted in a stable flame of 92 kW when the NRP discharge was applied at 30 kHz.

Moeck *et al.* [85] also explored a closed-loop control strategy in similar conditions ($\phi = 0.62$, $P_{\text{thermal}} = 41$ kW) exhibiting a TAI at 120 Hz. This time, the NRP discharges were operated with bursts of 30 kHz nanosecond pulses, with bursts triggered at various delays relative to the 8-ms pressure fluctuation period. The duration of each burst was about 4 ms, corresponding to a duty cycle of 50%. The effect of the NRP bursts on the acoustic pressure amplitude spectrum is shown in figure 14. Moeck *et al.* obtained the very interesting result that pressure oscillations could be either amplified or attenuated depending on the delay of the bursts. The maximum

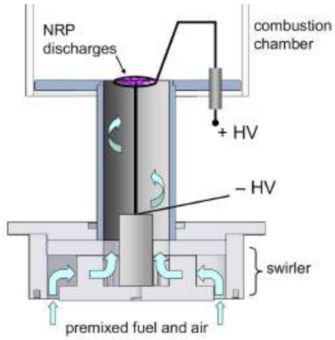

Figure 13: Experimental setup for TAI control in a premixed natural gas/air swirled flame at atmospheric pressure. The plasma is formed in a pin-to-ring configuration. Reproduced from Moeck *et al.* [85]

amplification and attenuation were achieved for delays of 2.2 ms and 6 ms, respectively. The strongest TAI attenuation was therefore obtained when the discharge bursts began near the minimum of the pressure oscillation, corresponding to a phase shift of about 75% of the pressure fluctuation period. They suggested that the active species generated by the discharge, mostly OH as discussed in section 2.2.1, increase the burning velocity, promoting oscillations of the burning velocity and hence of the heat release rate at the acoustic resonance frequency.

This closed-loop control strategy with gated bursts of pulses was later confirmed by [86] in a 230 W swirled laminar methane-air flame at atmospheric pressure stabilized by NRP glow discharges of about 1 W. Maximum attenuation was obtained when the bursts were exactly in phase opposition with the thermo-acoustic oscillations. However, they also showed that continuous forcing was just as effective in terms of actuation authority, for only 25% more plasma power.

Following these promising observations, several experiments were performed to control TAI in conditions closer to practical applications, *i.e.* (i) at high pressure up to 7 bar and (ii) for systems presenting large amplitude of pressure fluctuations.

First, demonstrations at higher pressures were made up to 4 bar in a swirl-stabilized flame [87, 88], and up to 7 bar in a dump combustor [89].

Second, the successful mitigation of large-amplitude TAI fluctuations at atmospheric pressure (1 to 4.5% of the mean pressure in the combustor, *i.e.* 1000 to 4500 Pa) was demonstrated by Kim *et al.* [90], Gomez del Campo *et al.* [14], and Shanbhogue *et al.* [22, 91]. All these experiments used NRP spark discharges with less than 1% of the flame thermal power (the flame power was up to 20 kW in these

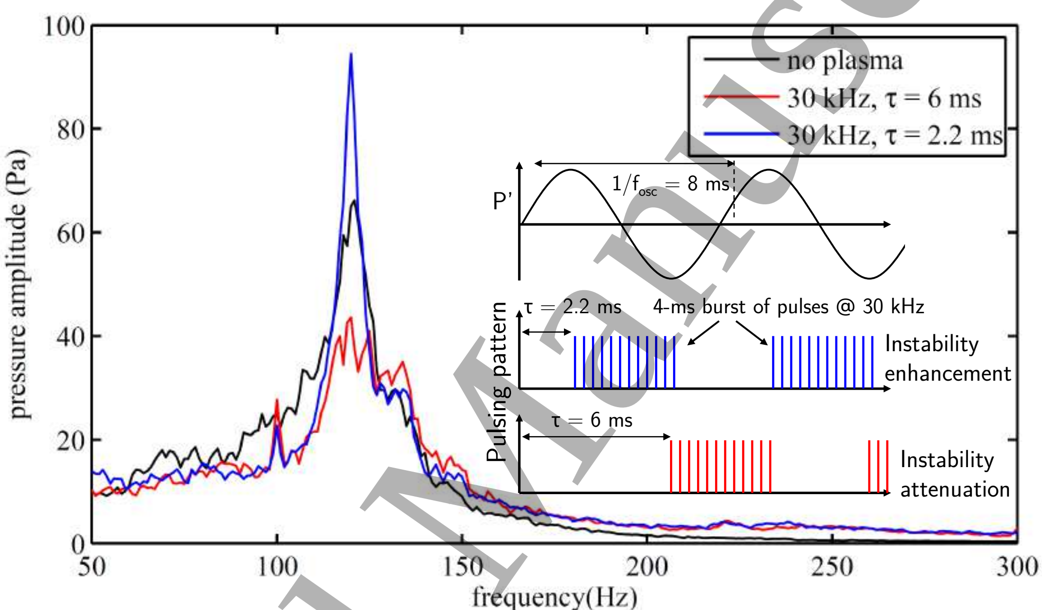

Figure 14: Mitigation and promotion of TAI in a swirled natural gas/air flame at P = 1 atm (P_{flame} = 41 kW, ϕ = 0.62). Pressure spectrum without discharge (black). Pressure spectra in the closed loop control cases, at maximum amplification (blue) and maximum attenuation (red) of the pressure oscillations. PRF = 30 kHz, P_{plasma} = 90 W. Adapted from Moeck *et al.* [85].

works). The discharges were applied continuously (not in burst mode) at the base of the flame, through the shear layers of the swirling flow, between a central electrode and the metallic combustor wall. In all cases, the TAI was strongly attenuated or nearly suppressed (factor 2 to 10 reduction of the peak pressure fluctuation amplitude). As shown by Pavan *et al.* [92], high-energy NRP sparks are more efficient at reducing the pressure oscillations than low energy streamers. Following this observation, Shanbhogue *et al.* [22] reduced the interelectrode gap of their previous work [91] to enforce the formation of sparks during each voltage pulse. With this modified setup, NRP discharge actuation was successful in *fully suppressing* instabilities across a wide range of equivalence ratios, with best reduction by as much as 23 dB, as shown in figure 15. Furthermore, Shanbhogue *et al.* [91] also devised an open-loop control strategy based on a reduced-order model to compute the acoustic fluctuations. They included the acoustic energy flux brought into the system by the discharges, describing it by an empirical function of the PRF. They then provided a simple state-space model to control the TAI by acting on the PRF. With this active control method, they were able to stabilize the flame at a set maximum fluctuation amplitude by adjusting the PRF.

These results are compiled in Table 2 along with other experimental demonstrations of TAI mitigation. As with LBO extension, these results were obtained for PRFs between 10-100 kHz and low plasma-to-flame power ratios (less than 1%).

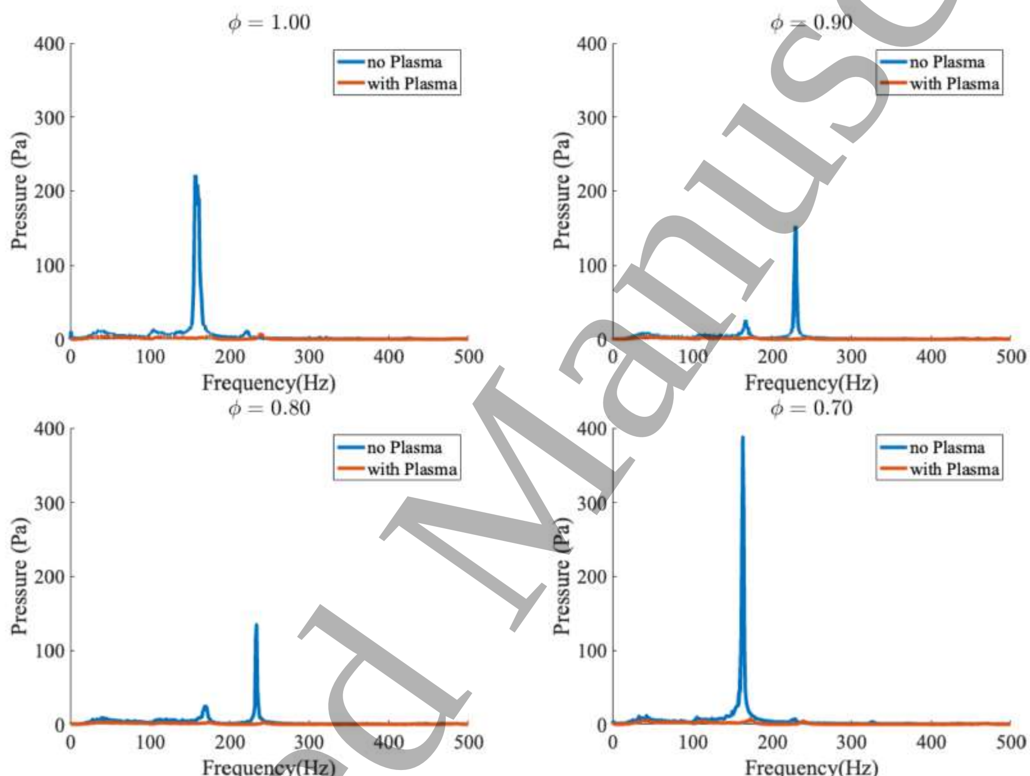

Figure 15: TAI suppression in methane-air flames at various fuel equivalence ratios with NRP sparks (8.64 mJ/pulse, PRF = 9 kHz, P_{plasma} = 78 W, P_{flame} = 6 kW, P = 1 atm). Reproduced from Shanbhogue *et al.* [22].

3.3 Mechanisms of thermo-acoustic instability mitigation

As seen in the previous examples, NRP discharges can help control TAI, either when applied in continuous mode or with bursts of pulses in phase opposition with the pressure fluctuations. It is interesting to understand how a continuously applied NRP discharge can help control TAI. Recent works have provided insight into this mechanism, as discussed below, but several open questions remain.

Pavan *et al.* [92] examined the discharges used in the conditions of the experiments of Shanbhogue *et al.* [91] with a 14-kW, atmospheric pressure, methane/air swirled combustor showing instabilities at 120-180 Hz. In these experiments, the discharges were produced at the base of the flame near the injector. When applied continuously, the discharges alternate between sequences of low-energy streamers (energy less than 100 μJ/pulse) and high-energy sparks (>13 mJ/pulse). The sparks are shown to occur during the minimum of the pressure oscillations in the flame (figure 7a in [92]). The sequence of spark pulses increases the HRR with a phase shifted from the pressure fluctuations, thus providing a stabilization source. However, the reason for the phase shift between the pressure and HRR fluctuations remains unexplained. It is likely the result of a complex two-way interaction between the flame and the plasma that requires further investigation [92,95]. The power deposited by the spark pulses can be controlled by adjusting either the pulse voltage or, for more flexibility, the pulse repetition frequency (PRF). Over the 3.5-ms duration corresponding to the half-period of positive HRR for a TAI at 140 Hz, 3 to 300 pulses can be deposited by varying the PRF from 1 to 100 kHz. This gives NRP discharges a considerable range of actuation authority.

Yu *et al.* [88] measured the FTF of a 3-bar swirled methane-air flame with and without NRP discharges. Without plasma, the 80-Hz heat release fluctuations at the top and bottom of the flame were measured to be in phase, whereas they were shifted by 180° once the plasma was applied (see Fig. 2 of [88]). Following the work of [96] who showed that stabilization is obtained when the angular oscillations of the bottom of the flame are in phase opposition with the flame vortex roll-up near the top of the flame, Yu *et al.* [88] suggest that the angular oscillations are affected by a plasma-induced increase in reactivity. However, the dependence of the phase shift on the plasma parameters remains to be explained. It would also be interesting to examine in future work how the flow velocity affects the stabilization process. Given that the flow velocity in the burner was 12 m/s and that the flame reached about half the combustion chamber height (which was 150 mm), the time for the perturbations generated at the base to reach the top of the burner is 6.25 ms. This time is exactly the half-period of the 80-Hz instability. A necessary condition for stabilization in these conditions might be that the convection time of the plasma-

Table 2: Experiments on thermo-acoustic instability control with NRP discharges (pulse duration = 10 ns). The last column in this table indicates the degree of attenuation of the thermo-acoustic instabilities. The overall sound pressure level (in decibels) is equal to SPL (dB) = $20\log(p_{\mathrm{rms}}/p_{\mathrm{ref}})$, with $p_{\mathrm{ref}} = 20\,\mu$Pa is the reference pressure level. NG stands for natural gas. The sequential burner of Dharmaputra 2023 and 2024 [81, 93] is further discussed in section 3.4.

Reference	Burner type	Fuel	P (bar)	P_{flame}	P_{plasma}	$\frac{P_{\mathrm{plasma}}}{P_{\mathrm{flame}}}$	PRF (kHz)	Instability frequency, amplitude	Reduction of TAI
Lacoste 2013 [84]	Swirled bluff-body	Methane ($\phi = 0.7$)	1	4 kW	40 W	1%	30	380 Hz, $u_{\mathrm{rms}} = 1.3$ m/s	Factor 10 on velocity fluctuation
Moeck 2013 [85]	Swirled	NG ($\phi = 0.66$)	1	43 kW	190 W, 315 W	0.44%, 0.7%	30, 50	150 Hz, 300 Pa	Factor 5, Factor >10
Moeck 2013 [85]	Swirled	NG ($\phi = 0.63$)	1	92 kW	190 W	0.2%	30	130 Hz, stable flame (< 100 Pa)	Increase of TAI up to 2200 Pa
Kim 2015 [90]	Dump (swirl)	Methane ($\phi = 0.8 - 0.95$)	1	6 kW	30 W	0.5%	15–30	150 Hz, 1000 Pa	25 dB (factor 18)
Gomez 2017 [14]	LDI	Methane ($\phi = 0.66$)	1	20 kW	< 200 W	< 1%	30	13 Hz, 2000 Pa	Factor >10
Kim 2021 [89]	Dump	Methane, Propane	7	20 kW	< 100 W	< 0.5%	5–110	200 Hz, 1600 Pa (at 5 bar)	6–12 dB (factor 2-4)
Shanbhogue 2023 [91]	Swirled	Methane ($\phi = 0.73$)	1	14 kW	120 W	0.9%	9	180 Hz, 4500 Pa	Factor 2 to 4
Shanbhogue 2024 [22]	Swirled	Methane ($\phi = 0.7$)	1	6 kW	78 W	1.3%	9	160 Hz, 1000 Pa	23 dB (factor 14)
Aravind 2024 [94]	Swirled bluff-body	Methane ($\phi = 0.75$)	2	11.6 kW	–	0.1–0.7, 0.4–1.4, 0.4–2.6	10, 30, 70	72 Hz, NA	TAI ×4 at low power, TIN ÷2 at high power
Dharmaputra 2023 [81]	Sequential burner	NG:H_2 (90:10%) ($\phi_g = 0.55$?)	1	73 kW	1.1 W	0.0015%	10–40	330 Hz, 4000 Pa	Factor 4
Dharmaputra 2024 [93]	Sequential burner	NG:H_2 (90:10%) ($\phi_g = 0.55$)	5.5	341 kW	29 W	0.008%	10	400 Hz, 15,000 Pa	Factor 3

induced perturbation is on the order of half the period of the TAI. This criterion would impact the electrode positioning in the chamber for TAI mitigation.

Finally, as shown in the experimental and numerical work of Malé *et al.* [68], further discussed in section 3.4 of this article, NRP discharges can produce plasma-heated pockets of gas, creating a sink term of acoustic energy. This sink term is advected to the unstable regions of the burner where it can balance the TAI oscillations.

In summary, plasmas can effectively reduce thermo-acoustic instabilities by inducing HRR fluctuations that are shifted relative to the phase of the thermo-acoustic fluctuations, both in open and closed loop actuation modes. The amount of energy deposited during an oscillation period can be easily varied over a wide range by adjusting the pulse repetition frequency. It should be noted that the electric field must be above the breakdown threshold, which is about 2.6 kV/mm/bar when the discharge is applied in gases at 300 K [97], and 0.5 kV/mm/bar when the discharges are applied in the flame (assuming a temperature of about 1800 K, typical of lean methane-air flames).

3.4 TAI mitigation in a model gas turbine combustor

We present in this section a demonstration of TAI control by NRP discharges in a high-power sequential combustor representative of staged energy gas turbines. The Constant Pressure Sequential Combustor (CPSC) is a recent breakthrough for ground-based gas turbines, allowing power generation with ultra-low NO_x emissions, improved operability, and fuel flexibility [98, 99]. Its great fuel flexibility is an asset for a quick decarbonation of power generation because conventional fuels can be directly replaced with new CO_2 neutral fuels (biofuels), CO_2 free fuels (hydrogen or ammonia), or mixtures of natural gases and hydrogen [81].

A schematic of the model CPSC operated at ETH Zurich at atmospheric pressure is shown in figure 16. The combustor is composed of two axially staged combustion chambers separated by an intermediate section, called the sequential burner where the hot gases issued from the first stage are diluted with cold air and where secondary fuel is injected. The second stage is operated in the lean regime. The primary interest of air dilution upstream of the sequential burner is to cool the hot gases exiting the first stage down to a temperature slightly below the autoignition temperature, thus delaying autoignition of the second stage while allowing the fuel injected in the sequential burner to fully mix with the air-diluted flame products and prevent the formation of fuel-rich pockets. The flow entering the second-stage combustion chamber is then a well-premixed lean mixture whose combustion produces very low

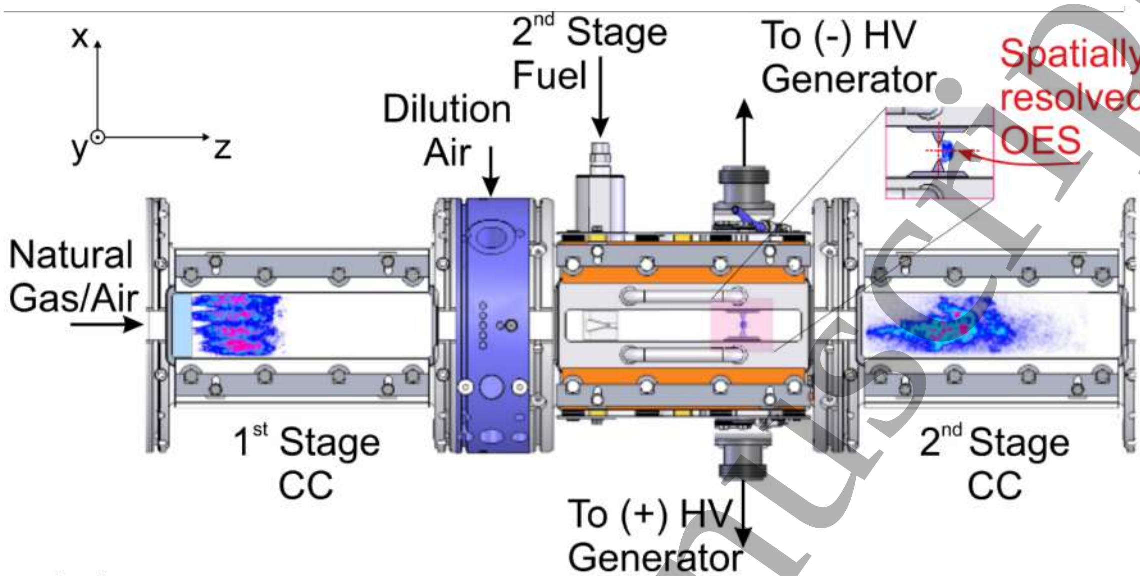

Figure 16: Schematic of the model Constant Pressure Sequential Combustor operated at ETH Zurich. Reproduced from Shcherbanev *et al.* [100].

NO_x emissions.

In practical operation, however, the CPSC faces two major issues that PAC seeks to address. First, LBO may occur if the operating conditions change rapidly. Second, TAI inherent to lean flames may develop in the two stages of the combustor. Recently, several experimental studies were conducted in this combustor to address these two issues. In these experiments, the first stage was injected with a lean mixture ($\phi = 0.8$) of natural gas (0.7 g/s) and air (15 g/s), producing a 35-kW flame. The hot gases were then diluted with air (18 g/s) to decrease the mixture temperature to about 1000 K, *i.e.* just below the auto-ignition temperature. A mixture of natural gas (NG) and hydrogen, with mass fractions varied from a comparatively low reactivity fuel (LR) with 1.5% H_2/98.5% NG, to a high reactivity fuel (HR) with 20% H_2/80% NG, was injected in the second stage. The global flow rate of the fuel was adjusted to keep an overall fuel equivalence ratio close to 0.6 and thus a flame thermal power around 37 kW in the second stage. The total thermal power in the CPSC was 72 kW for all conditions.

A first beneficial effect of NRP discharges on flame ignition and stabilization was demonstrated in [100]. Under the LR conditions without plasma, no ignition was obtained in the second stage. However, it was possible to ignite and stabilize the flame with NRP spark discharges of mean power 350 W (7 mJ/pulse at 50 kHz,

$V = 16.5\,\text{kV}$, gap distance of 5.1 mm, 0.5% of the flame thermal power). For the HR conditions, the flame without plasma ignited and stabilized near the entrance of the second stage. In that case, even a very low power NRP *glow discharge* of only 14 W (0.28 mJ/pulse at 50 kHz, $V = 10.5\,\text{kV}$, 0.02% of the flame thermal power) was sufficient to stabilize the flame. NRP *spark discharges* were more effective in accelerating combustion, but they moved the ignition too far upstream into the sequential burner, which is detrimental to NO_x emissions as the fuel is not fully premixed at the autoignition point. In summary, the LR flame can be stabilized with about 0.5% of the flame thermal power, a typical value for PAC, and the HR flame with a very low 0.02%, showing that blending H_2 with natural gas considerably decreases the plasma power requirements.

A second beneficial effect regarding the suppression of TAI was recently demonstrated in an experimental and numerical LES study by the same group [68]. The experimental conditions were close to those of the previous case, except that only the HR case was studied. The NRP discharges had an ultra-low mean power of 3.56 W (3.56 mJ/pulse at 10 kHz, $V = 9\,\text{kV}$, gap distance = 8 mm, 5×10^{-3}% of the flame thermal power). Without plasma, a strong TAI at 308 Hz with a pressure fluctuation amplitude of about 4 kPa appeared in the combustor. With plasma, the TAI was almost entirely suppressed, as shown in figure 17.

Through LES of this experiment, Malé *et al.* [68] and Impagnatiello [101] showed that the NRP discharges generate HRR fluctuations (q') in phase opposition to the pressure fluctuations (p') in the sequential burner. Comparing OH* emission imaging and LES, they showed that the HRR fluctuations are due to the creation in the mixing section of periodic ignition kernels in phase opposition with the pressure fluctuations in that region, see figure 18. The periodic ignition kernels are then convected toward the second stage. This effect creates a sink term in the acoustic energy balance equation that dampens the thermo-acoustic instability in both the first and second stage combustion chambers, as shown in figure 19. The response time of plasma-induced stabilization was found to be about 30 ms.

As already mentioned in section 2, the choice of plasma parameters is extremely important for stabilization. Dharmaputra *et al.* (figure 3 of [81]) showed that pulses at 12.5 kV with the same average power deposited of 3 W (10 kHz @ 0.3 mJ/pulse and 40 kHz @ 0.08 mJ/pulse) have an opposite effect on the main TAI at 308 Hz and on a secondary TAI at 260 Hz. In both cases, the main TAI is reduced. However, the secondary TAI is suppressed at 10 kHz, whereas at 40 kHz it is amplified. This effect was reproduced with LES by [101]. This shows again that NRP discharges can either stabilize a thermo-acoustically unstable system, or destabilize a stable one.

The key effects of the PRF and applied voltage are further discussed by Dharma-

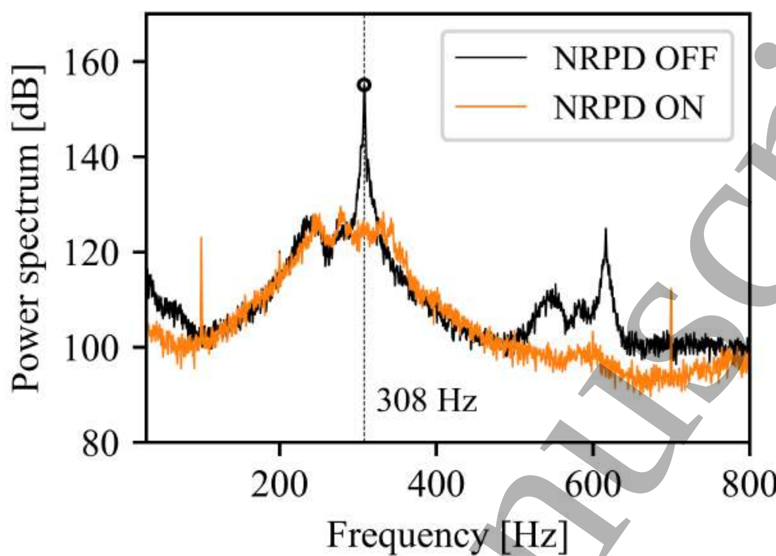

Figure 17: Power spectrum of the acoustic pressure in the first stage combustion chamber normalized with a reference pressure of 20 µPa, with and without NRP discharge. The amplitude peak at 308 Hz is successfully suppressed by the NRP discharges. P_{flame} = 73.4 kW, P_{plasma} = 3.6 W. Reproduced from Male *et al.* [68].

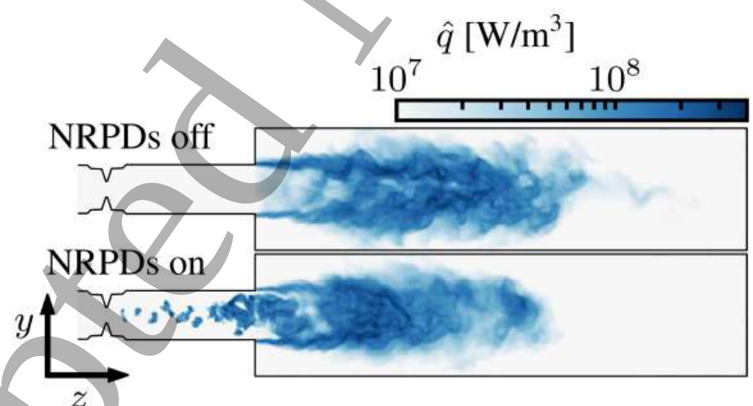

Figure 18: Planar cuts of the instantaneous averaged heat release rate without (top) and with (bottom) NRP discharges. The periodic ignition kernels created by the discharge are convected toward the sequential combustion chamber and stabilize the TAI. Reproduced from Impagnatiello *et al.* [101].

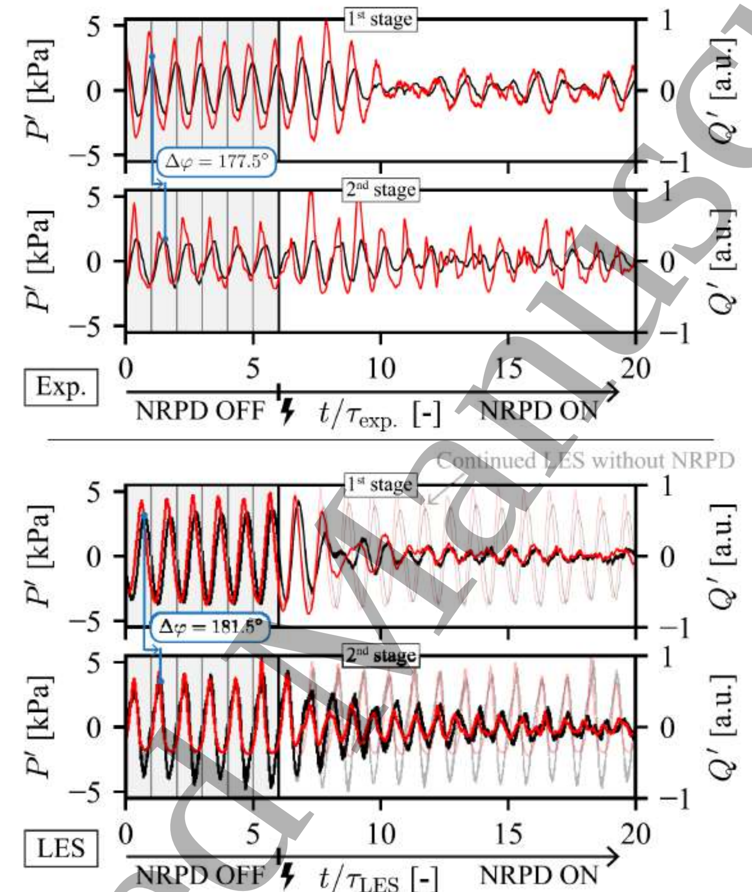

Figure 19: Fluctuations in pressure (black lines) and volume-averaged heat release (red lines) in the first and second stages for both experiments (top) and LES (bottom) under application of NRP discharge. The faint lines correspond to a continuation of the LES without plasma. The time abscissa is normalized by the period of the instability in the experiment ($\tau_{\mathrm{exp}} = 1/308$ Hz ≈ 3.25 ms) and in the simulation ($\tau_{\mathrm{sim}} = 1/324$ Hz ≈ 3.09 ms). Reproduced from Male *et al.* [68].

putra *et al.* in [81]. First, they note that stabilization is not possible below a threshold electric field (about 2.2 kV/mm in their conditions), whatever the PRF. Above that threshold field, the PRF should be adjusted so that the q' produced by the discharges is sufficient to control the TAI. However, above a certain value of the PRF, the discharges increase the NO_x levels. In the experiments of Malé *et al.* [68], low PRFs around 10 kHz were sufficient to stabilize the TAI without increasing the NO_x levels. At 40 kHz, the NO_x penalty significantly increased (factor 2). Dharmaputra *et al.* [81] attributed this strong increase to the change in morphology of the discharge. At 10 kHz, the discharge appears as a single filament along the interelectrode axis. At 40 kHz, the discharge bends along the axis of the flow, which can be attributed to the convection of the heated channel not too far from the interelectrode axis and the next pulse following a path in this heated channel [100]. The synergy between the multiple pulses strongly enhances the heat release, leading to increased NO_x formation. Thus, the pulse frequency must be carefully chosen.

In addition, the PRF also has a strong influence on the probability of development of an ignition kernel by a sequence of consecutive pulses. As shown by Lefkowitz, Ombrello and co-workers [102–106], depending on the flow velocity and pulse repetition frequency, the ignition kernels may be either fully coupled, partially coupled, or fully decoupled, as a result of constructive or destructive interferences. These interferences were explained numerically by Tanaja *et al.* [64], using LES simulations with the phenomenological model of Castela *et al.* In the partially coupled regime, [64] showed that the shock wave produced by a pulse convectively cools the plasma created by the previous pulse, thus reducing the ignition probability. This effect also depends on the gap distance, the energy deposited by each pulse, and the flow velocity. As a result, the operating parameters of the discharge must be carefully optimized.

Finally, in recent work, Dharmaputra *et al.* [93] experimentally succeeded in controlling a 400-Hz TAI in a 343-kW CPSC at pressures up to 5.5 bar, with a fuel blend of 90% natural gas and 10% hydrogen, and with only 0.008% of the flame thermal power.

In summary, NRP discharges have been shown to successfully reduce TAI in representative combustion systems. The key parameters include the reduced electric field (which must be close to breakdown), the pulse repetition frequency (high enough to deposit enough energy, but low enough to prevent excessive NO_x formation), and the residence time from the discharge to the combustion chamber. However, the dependence of the FTF to these parameters remains to be explained. Fortunately, there is now sufficient fundamental knowledge to model these phenomena and carry out numerical simulations to design optimal actuation strategies. These advances now open the way to demonstrations in high-power, high-pressure combustors.

4 Pollutant emissions

As already mentioned, reducing pollutant emissions is a major issue in combustion applications. Several agencies provide regulations to control the various pollutants: for aviation, the International Civil Aviation Organization (ICAO) currently provides a set of regulations described by CAEP/8 [107]. The strategy to burn fuels in a well-premixed lean regime offers many advantages, namely the reduction of NO_x thanks to the lower flame temperatures, and the reduction of soot and unburned hydrocarbons (UHC) thanks to the higher fraction of oxidizer. However, when plasma discharges are applied in lean flames, they create radicals and heat that can in turn adversely affect the formation of pollutants.

4.1 Experimental observations and mitigation strategies

4.1.1 Hydrocarbon-air flames

A detailed study on the formation of pollutants (NO_x, CO) in a swirl-stabilized lean methane-air flame was conducted by Kim *et al.* [23]. They used DBD discharges (at 7 kV and 4 kHz) with a plasma power of 1-2% of the thermal flame power to extend the stability and LBO limits. The effect of the discharge on the concentrations of CO and NO_x was measured as a function of the fuel equivalence ratio. Their results are shown in figure 20. Without plasma, CO and NO_x follow the same trends as previously highlighted in figure 7, *i.e.* a decrease of NO as the fuel equivalence ratio decreases, and an increase of CO when the fuel equivalence ratio approaches the LBO limit. With plasma, the LBO limit is extended by about 10%, from $\phi = 0.56$ to $\phi = 0.50$. In addition, with plasma the increase in CO occurs at a lower equivalence ratio and the peak emission is twice lower than without plasma. This demonstrates that plasma can be used not only to increase flame stability, but also to reduce CO emissions. However, the DBD discharge also induces a strong penalty on the emissions of NO (figure 7b).

It is interesting to note that NO_2 represents less than 1% of the total NO_x produced in NRP discharges, the rest being NO [19, 22]. Malé *et al.* [67] performed numerical simulations of NO_x production in the CPSC, using a NO_x/combustion chemistry mechanism with the phenomenological model of Barleon *et al.* [62]. The results were found to be in good agreement with the measured NO concentrations, and the plasma-induced NO increase was primarily attributed to the reaction $N(^2D)+O_2 = NO + O$.

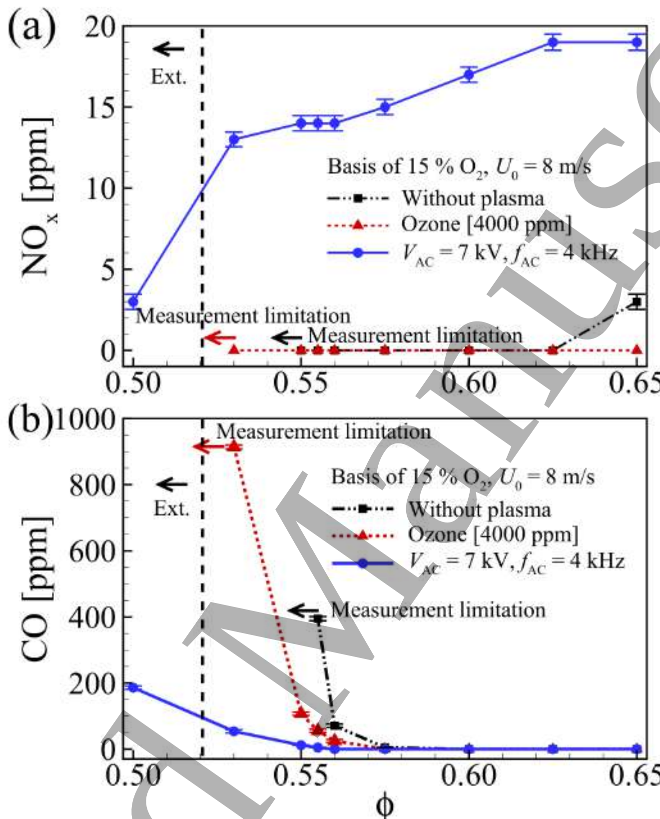

Figure 20: Effect of DBD on LBO extension in a swirl-stabilized methane/air flame at P = 1 atm. The DBD extends the LBO limit from $\phi = 0.56$ to $\phi = 0.50$. (a) NO_x emissions significantly increase at relatively high plasma-to-flame power ratios (1-2%) in the DBD-stabilized flame. (b) The CO emissions, on the other hand, are largely reduced near the LBO limit. By comparison, O_3 addition has less effect on the LBO extension and CO emissions, but a negligible penalty on NO_x emissions. Reproduced from Kim *et al.* [23].

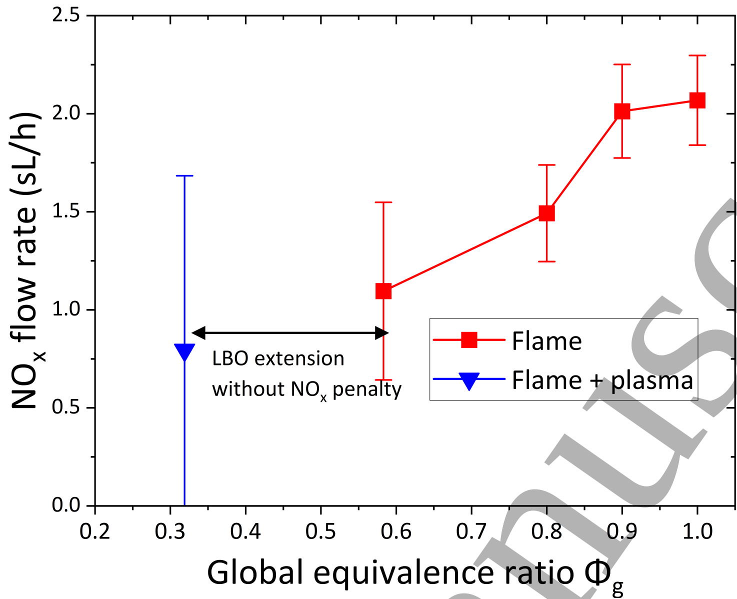

Figure 21: LBO extension and NO_x emissions as a function of the BIMER-PAC global fuel equivalence ratio (keeping $\dot{m}_{CH_4}$ constant). $P_{\text{flame}} = 50$ kW, $\alpha_p = 80\%$, $P_{\text{plasma}} = 0.6\% \times P_{\text{flame}}$. Adapted from Blanchard *et al.* [110].

The production of NO_x in plasma-assisted flames is highly sensitive to the plasma discharge power. Several studies with laboratory combustors [19,21,81,84,90,108,109] have shown that the concentration of NO increases linearly with the plasma power, and that even with only 1% of the flame thermal power, the NO_x penalty is already significant.

To keep the NO_x penalty to a low level, plasma power mitigation strategies must be used. A trade-off must thus be found between producing enough active species to stabilize the flames while limiting the production of NO_x. A promising strategy, proposed by Blanchard *et al.* [19], consists in applying NRP discharges in burst mode, with a carefully selected sequence of on- and off-pulses. With this method, they were able to significantly extend the LBO limit of a 50-kW methane-air flame in the BIMER-PAC facility without NO penalty, as shown in figure 21. Interestingly, the lowest NO_x penalties reported in the literature were obtained with a plasma power less than 0.1% of the flame thermal power [19, 26, 81].

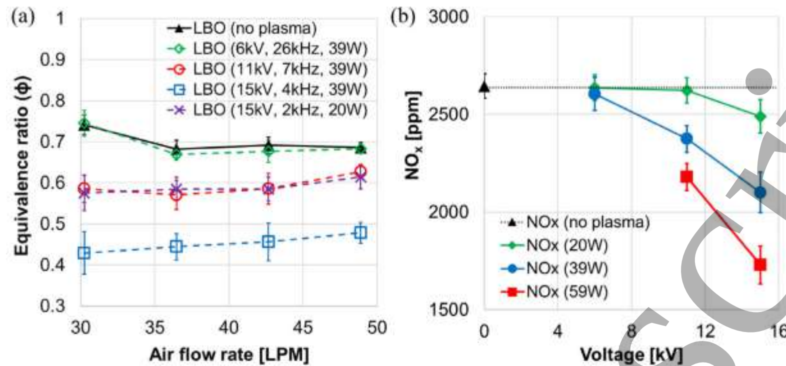

Figure 22: (a) Lean blow-off limits of ammonia/air flames with and without plasma, (b) NO_x emissions without and with plasma ($\phi = 0.94$). Reproduced from Choe *et al.* [18].

4.1.2 Hydrogen-air flames

Under stoichiometric conditions, hydrogen-air flames produce high NO_x concentrations (via the thermal Zeldovich reactions) because their adiabatic temperature is higher than hydrocarbon-air flames. However, for applications of interest, hydrogen flames can be operated in very lean regimes (fuel equivalence ratio typically < 0.3) where NO_x emissions are low. As for hydrocarbon flames, plasma can extend the LBO limit but this comes at the expense of an increase in NO_x emissions, even though this increase can be limited by applying pulses in burst mode [21].

4.1.3 Ammonia-air flames

The NO_x emissions of ammonia-air flames follow a very different trend than in hydrocarbon-air or hydrogen-air flames. Instead of peaking near stoichiometric conditions, NO_x emissions in ammonia flames can have their maximum in lean conditions [111]. This is because the main mechanism of NO_x production is no longer the thermal Zeldovich mechanism, but instead the so-called fuel-bound mechanism where the nitrogen atoms forming NO come from the fuel itself. Plasmas have been found to be effective for both LBO extension and NO_x reduction [18, 112, 113]. It should be noted that plasmas have very different effects on NH_3 flames than on hydrocarbon or hydrogen flames. Whereas for hydrocarbon flames increasing discharge power improves LBO limits but worsens NO_x emissions, for NH_3 flames increasing discharge power or voltage offers the benefits of both improved flame stability and NO_x reductions, as shown in figure 22

4.2 Mechanisms of NO_x formation in PAC

There are several possible routes for the formation of NO in plasma-assisted flames. First, the plasma may increase the gas temperature and the concentration of O, N, or OH radicals, which enhance the formation of NO via the Zeldovich reactions [114]:

$$N_2 + O \rightleftharpoons NO + N \tag{5}$$

$$N + O_2 \rightleftharpoons NO + O \tag{6}$$

$$N + OH \rightleftharpoons NO + H \tag{7}$$

Second, NO can be formed via dissociative quenching reactions involving excited electronic states of N_2 and N, which are formed by electron-impact excitation and dissociation of N_2. We term these reactions the "excited Zeldovich reactions":

$$(a) \quad N_2^* + O \rightarrow NO + N \quad k_{fa} = 3 \times 10^{-10} \text{ cm}^3/\text{s} \tag{8}$$

$$(b) \quad N(^2D) + O_2 \rightarrow NO + O \quad k_{fb} = 1.5 \times 10^{-12} \left(\frac{T}{300}\right)^{0.5} \text{ cm}^3/\text{s} \tag{9}$$

The rate constant of reaction (a) is based on measurements and simulations of O, N, and NO densities in the afterglow of a nanosecond discharge [115, 116]. Shkurenkov *et al.* attempted to explain the high NO densities measured in their experiments by assuming a near kinetic rate for the quenching reactions involving the following excited electronic states of N_2: $B^3\Pi_g$, $B'^3\Sigma_u^-$, $W^3\Delta_u$, $C^3\Pi_u$, $E^3\Sigma_g^+$, $a'^1\Sigma_u^-$, $a^1\Pi_g$, $w^1\Delta_u$, $a''^1\Sigma_g^+$. However, further work is needed to confirm these mechanisms of NO formation by nonequilibrium discharges.

For ammonia-air flames, the pathways of NO_x formation and depletion are quite different than with hydrocarbons or hydrogen. First, as already mentioned, NO is mainly formed from fuel-bound nitrogen atoms. In addition, discharges can also decrease NO_x via reducing reactions. This was observed by Choe *et al.* [18] in ammonia-air flames where the NRP discharges led to a strong decrease in NO emissions. Compared to the 2650 ppm observed at $\phi = 0.94$ in the non-assisted flame, NO concentrations were found to decrease with increasing plasma power, down to about 1700 ppm at the highest plasma power in their study. Choe *et al.* attributed this reduction to two potential reaction pathways: 1) The HO_2 formed in the plasma region can react with NO and NO_2 through reactions:

$$NO + HO_2 \rightarrow OH + NO_2 \tag{10}$$

$$NO_2 + HO_2 \rightarrow HONO + O_2 \tag{11}$$

2) NO is consumed by reactions with NH_2:

$$NO + NH_2 \rightarrow NNH + OH \tag{12}$$

$$NH_2 + NO \rightarrow N_2 + H_2O \tag{13}$$

which are the key reactions of the thermal de-NO_x process [117]. For detailed reviews on NO_x formation/depletion mechanisms in plasma-assisted ammonia-air flames, the reader is referred to the articles of Shah *et al.* [118] and Mao *et al.* [119].

5 Enhancement of supersonic combustion

5.1 Supersonic combustors

Another active field of plasma-assisted combustion is the enhancement of supersonic combustion to fly at hypersonic speeds (Mach > 5). Air-breathing hypersonic aircraft use a scramjet engine, as illustrated in figure 23. The inlet air ($\approx$ Mach 5) is slowed down to supersonic speed (typically Mach 2) via a specially shaped duct. Then, fuel is injected, mixed and burned in a constant or slightly diverging area section. The burned gases exhaust through an expanding nozzle to provide thrust. The challenge has often been compared to "lighting a match in a hurricane and keeping it lit for 30 minutes".

The typical flight corridor of hypersonic aircraft is shown in figure 24. At low altitudes, atmospheric drag becomes important, which limits the propulsion efficiency, and the high degree of air compression may cause excessive heating leading to structural damage. At high altitudes, the flame blows off because of the low atmospheric oxygen density and low pressure conditions inside the combustor.

Several flight tests of scramjets were conducted in the past 20 years (figure 25). In 2004, under the Hyper-X program, NASA conducted two successful flight experiments with a hydrogen-air scramjet engine: the X-43A vehicule launched in March 2004 operated for 11 s and reached Mach 6.83, and the following attempt in November 2004 flew for about 10 s and reached Mach 9.68. Soon after, the US Air Force conducted the X-51A series of flight experiments (HyTech program) with a scramjet operating with JP7 fuel. The objective was to launch the vehicle from a B-52 aircraft, to accelerate it to Mach 4.8 with a booster rocket, and to reach Mach 6 with the scramjet after separation from the booster. On the fourth attempt in 2013, X-51A accelerated to Mach 5.1 and flew for 210 s, thus demonstrating the transition from subsonic to supersonic combustion and breaking the record for the longest-duration hypersonic flight experiment. Although the vehicle did not reach the target velocity of Mach 6, the program provided a wealth of experience for future missions.

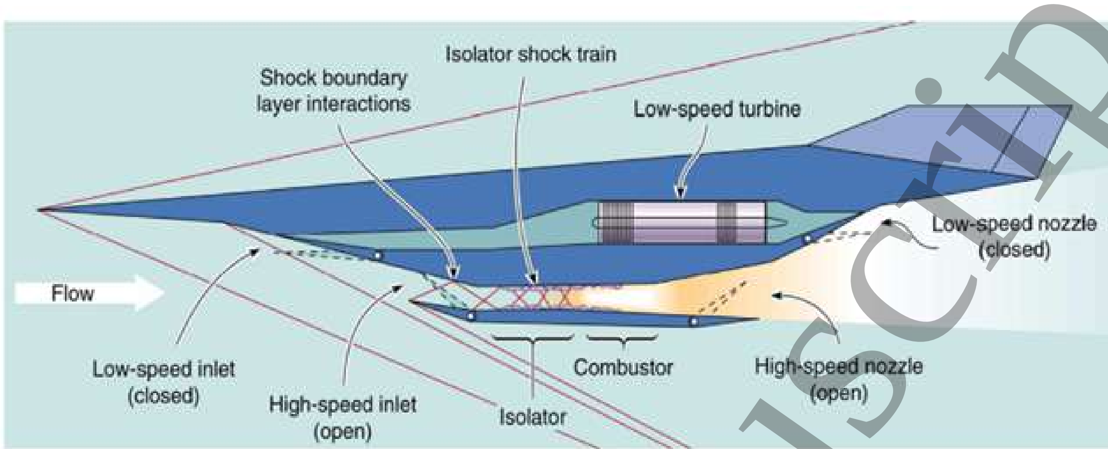

Figure 23: Schematic of a scramjet engine as part of a Turbine Based Combined Cycle (TBCC) engine. The turbine is used to accelerate the vehicle from take-off to Mach ≈ 3, then the dual ramjet/scramjet engine (bottom part) takes over with a transition from ramjet to scramjet mode at flight Mach numbers between 5 and 6. Reproduced from [120].

Comprehensive reviews of research and flight experiments with scramjet engines, along with challenges and mitigation strategies, can be found in several reviews such as those of Leonov (2018) [123], Cai *et al.* [124], Yu *et al.* (2020) [29] and Lv *et al.* (2022) [125]. Leonov [123] identifies three main areas where plasmas can help improve the operation of scramjet engines. These include (1) plasma-assisted ignition, and (more importantly) flame holding, in conditions where the fuel-air temperature is below the self-ignition threshold, (2) fuel-air mixing intensification, and (3) enhancement of combustion in the transition regime from ramjet to scramjet operation, and control of combustion instabilities. As indicated on figure 24, plasma assistance may be most useful in the range Mach 5-6, where the transition from subsonic to supersonic speed leads to a significant decrease of the static temperature and of the fuel-air mixing efficiency. In addition, plasma can help extend the flight corridor to higher altitudes, which has the advantage of reducing the environmental footprint of water emission in the stratosphere, as the photochemical lifetime of water decreases by a factor 3 between the altitudes of 30 and 35 km [121].

The reviews of Leonov [123] and Cai [124] provide extensive overviews of the various plasma solutions investigated by research teams around the world. Some of the early efforts used DC plasma torches to inject an ionized fuel mixture into the crossflow of incoming air, and showed effective ignition at velocities up to about

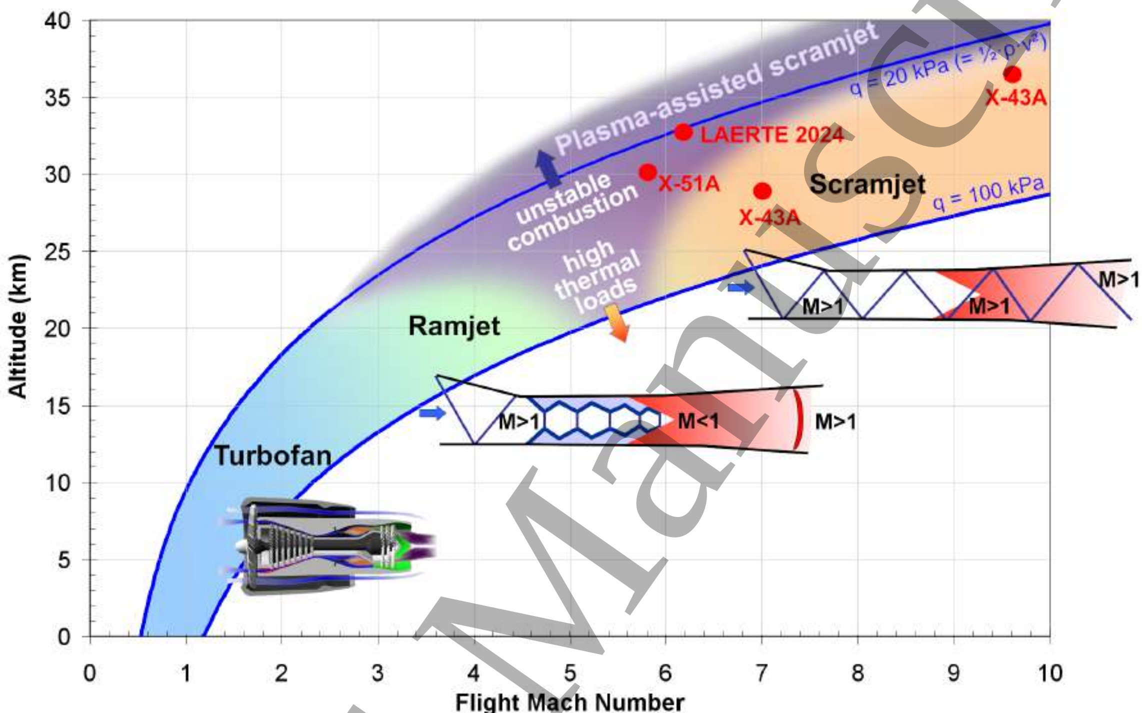

Figure 24: Flight domain of air-breathing vehicles. Regions where PAC may be the most effective correspond to the high-altitude range and to the transition from ramjet to scramjet operation around Mach 5-6 (purple area). q is the dynamic pressure, $q = \frac{1}{2}\rho v^2$. The LAERTE point corresponds to the experiments of Vincent-Randonnier *et al.* [121]. For reference, the highest velocities reached by the two successful X-43A flight experiments (hydrogen-fueled) were Mach 7 at 28.5 km altitude (March 2004) and Mach 9.6 at 36.3 km (November 2004). The X-51A Waverider (JP7-fueled) reached Mach 5.1 at 21 km altitude May 2013. Adapted with Axel Vincent-Randonnier from [122].

Figure 25: X-43A Hypersonic Experimental Vehicle (this image is stated to have been released into the public domain. It is included within this article on that basis.) and X-51A Waverider hypersonic flight demonstrator (this X-51A Waverider, U.S. Air Force graphic has been obtained by the authors from the Wikimedia website, where it is stated to have been released into the public domain. It is included within this article on that basis.).

100 m/s. To operate at the higher speeds of scramjets, researchers have focused on nonequilibrium filamentary discharges produced between electrodes mounted flush to the surface of the duct.

An example from the Stanford group [126] is shown in figure 26. Sonic or subsonic jets of hydrogen are injected through flush-mounted nozzles into an oxygen crossflow at M = 1.7–2.3. A plasma created by a 50-kHz NRP discharge is used to ignite the hydrogen-oxygen flame. The electrodes are also flush-mounted to minimize stagnation pressure losses inside the duct. Flame ignition is obtained in a configuration combining an upstream subsonic oblique jet and a downstream sonic transverse jet.

Leonov and co-workers [122, 123, 127–129] investigated the use of near-surface, quasi-DC discharges between flush-mounted electrodes positioned upstream or downstream of the fuel injector, as shown in figures 27a-b. They later found that better results were obtained when the quasi-DC discharges were co-located with the fuel injector, as shown in figure 27c. In this latter configuration, called Plasma-Injection Module (or PIM), 100-mm long plasma filaments propagate into the crossflow (figure 28). The advantage of this configuration is that the discharge chemically activates the fuel and promotes mixing with the air flow via the streamwise vortices (figure 28b) induced by thermal inhomogeneities in the fuel jet. The filamentary channel was characterized as a weakly nonequilibrium plasma (temperature around 3000–6000 K, electron density around $10^{15} - 10^{16}$ cm^{-3}, reduced electric field around 10 Td) producing large amounts of radical species [127]. The filament propagates into the flow up to a length of about 10 cm, and periodically restrikes at frequencies on the order of a few kHz. Although the importance of nonequilibrium chemistry was shown to

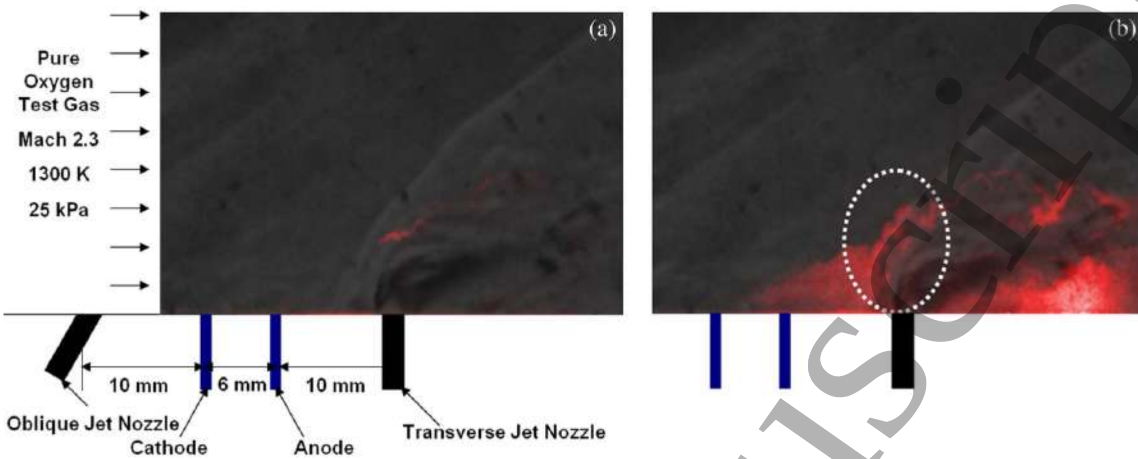

Figure 26: OH PLIF images (red) superposed with a typical schlieren image at the same flow conditions (a) without plasma (b) with plasma (reproduced from [126]).

be more significant than the thermal effects, the relative importance of combustion enhancement by the produced radicals and by the enhanced mixing is still an open question.

Braun *et al.* [130] studied a Q-DC discharge setup with 4 PIM modules inspired from the setup of Leonov *et al.* in a high-power (1-2 MW) ethylene-air scramjet operating at a stagnation temperature and pressure of $T_0 = 475$ K and $P_0 = 240$ kPa. It should be noted that the PIMs had to be located downstream of the cavity and that the spatial extent of the gliding arcs was fairly short due to thermal and geometrical constraints. Although the effects were limited to a narrow range of non-optimal burning conditions, the authors were able to push the system past the threshold of heat release required to transition from scram-mode to ram-mode with $\sim$8 kW of PIM power ($<$ 1% of the thermal power of the scramjet). A similar effect was obtained by flowing additional fuel, but in that case the required thermal power was higher ($\sim$12 kW), demonstrating that the PIM system is more effective than fuel addition to promote the transition.

Another widely studied configuration is the non-thermal multi-channel gliding arc (MCGA) plasma. Several studies in cavity-based supersonic combustors have shown the MCGA ability to enhance ignition and combustion [131], and to suppress combustion mode transitions [132].

Ombrello *et al.* [134] demonstrated enhanced ignition and combustion in an ethylene-air cavity at Mach 2 using nanosecond-pulsed high-frequency discharges (NPHFDs) at PRFs in the range 1.5-300 kHz. Ignition was obtained over a wide

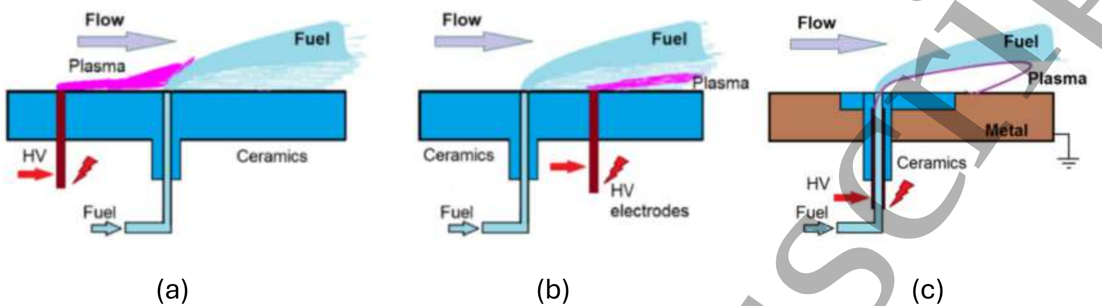

Figure 27: Three configurations studied by Leonov and co-workers: (a) electrode upstream of fuel injection, (b) electrode downstream of fuel injection, (c) electrode co-located with fuel injection (reproduced from from Leonov [123]).

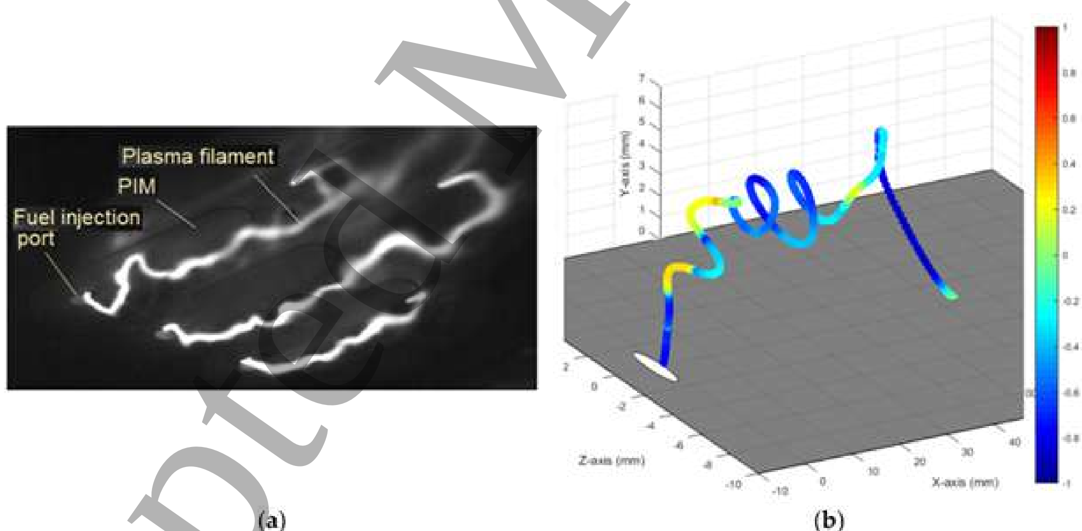

Figure 28: Filaments created by 3 PIM modules in the experiment of Leonov *et al.* (reproduced from Leonov *et al.* [128]).

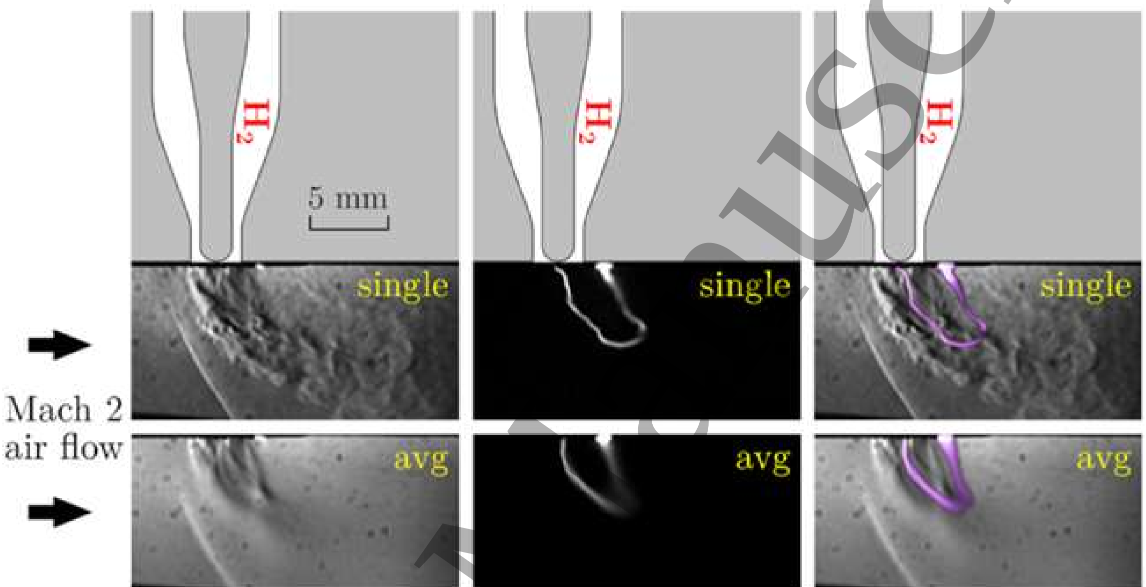

Figure 29: Flush-mounted Plasma/H_2-injector module producing a quasi-DC arc discharge in a supersonic air crossflow at Mach 2 ($p_0 = 0.413$ MPa, $T_0 = 1538$ K) in the LAPCAT2 Dual Mode Ramjet combustor at the LAERTE facility of ONERA. Hydrogen jet conditions: $p_0 = 0.760$ MPa, $T_0 = 303$ K, jet-to-crossflow momentum ratio: $J = 2.00$). The crossflow conditions are close to the minimum self-ignition temperature at 0.4 MPa. Global fuel-equivalence ratio: $\phi = 0.18$. Plasma power: 1.4 kW. Left column: instantaneous and averaged Schlieren images of the flow. Middle: photographs of the gliding arc. Right: superposition of Schlieren and discharge images (reproduced from Vincent-Randonnier *et al.* [121]).

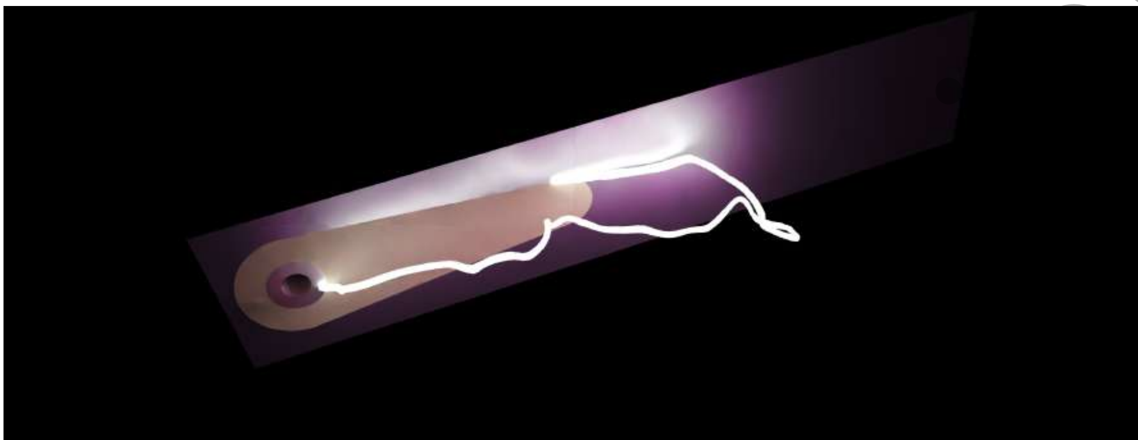

Figure 30: 3D numerical simulation of the filamentary arc produced by a PIM module and convected by the flow in the LAERTE facility. The contour of the white area is the 5000 K isotherm. The simulation corresponds to the instant when the arc is fully extended, just before restrike. Adapted from Rocamora *et al.* [133].

range of fuel equivalence ratios and with five times less power than with a traditional capacitive spark discharge. They attributed the improved performance to the production of large amounts of O radicals and to the synergy between successive pulses.

An alternative configuration to the PIM system of Leonov *et al.* was recently developed by Vincent-Randonnier *et al.* [121] for the LAPCAT2 Dual Mode Scramjet combustor of the LAERTE facility at ONERA. Hydrogen is injected into a supersonic air crossflow (Mach 2) through a nozzle containing a coaxial high voltage electrode. The coaxial injection module is mounted flush with the LAPCAT2 chamber's wall. A quasi-DC discharge is produced between the central electrode and the wall of the combustor. The plasma filament extends a few centimeters into the crossflow (figure 29), with periodic restrikes as in a gliding arc. The crossflow conditions are around the minimum self-ignition temperature (T_0 = 1490 K at p_0 = 0.41 MPa). The static pressure inside the chamber is about 0.06 MPa. These conditions correspond to a flight Mach number of 6.25 and an altitude of 32.5 km, as indicated by the point noted LAERTE on figure 24. In a first series of tests with a plasma power of about 1.4 kW, combustion was significantly enhanced as seen from the photographs and pressure traces of figure 31. In recent unpublished work, Vincent-Randonnier, Pilla, and Labaune (private communication 2025) decreased the stagnation temperature below the minimum self-ignition threshold and increased the plasma power up to about 3 kW. In these conditions, they succeeded in sustaining combustion with the

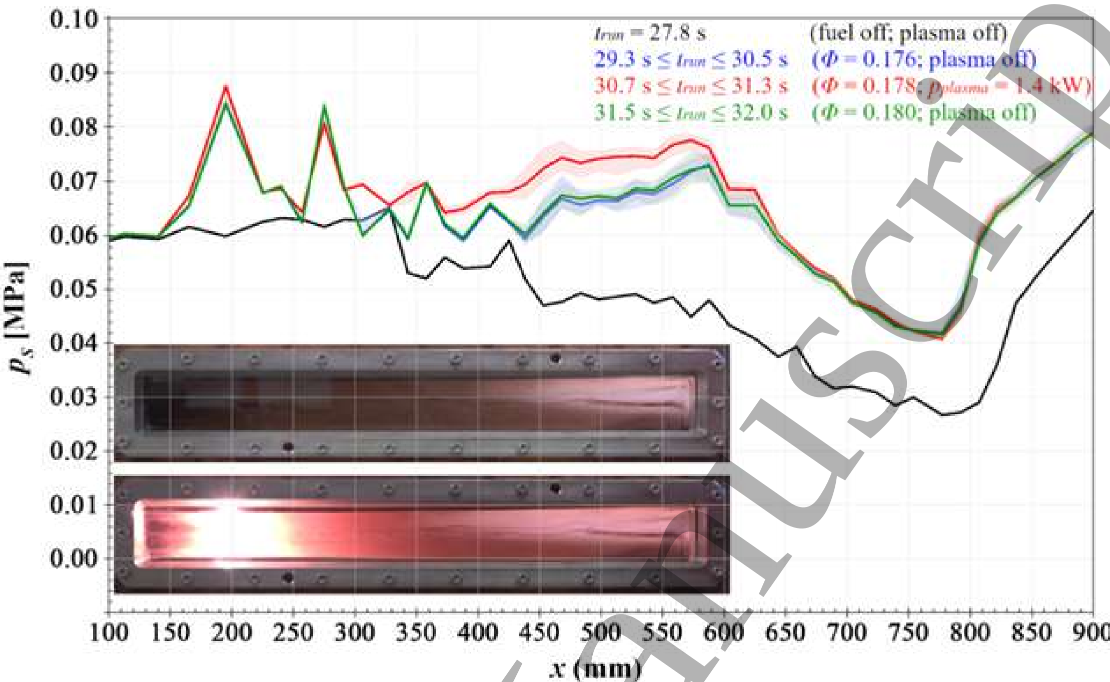

Figure 31: Pressure profile along the LAERTE combustor before fuel injection (black line) and at $\phi = 0.18$ before (blue), during (red) and after (green) plasma activation. $p_0 = 0.41$ MPa, $T_0 = 1490$ K, $\dot{m}_{air} = 316$ g/s, $\dot{m}_{H_2} = 1.7$ g/s). Inset: photographs of supersonic combustion without plasma (top) and with plasma (bottom). Reproduced from Vincent-Randonnier *et al.* [121].

plasma on, whereas ignition was not possible without plasma. The plasma power was less than 1.8% of the thermal power of the supersonic flame, estimated to be around 160 kW.

In recent work, Rocamora *et al.* [133] performed the first LES of H_2-air ignition and combustion sustainment at Mach 2 with a PIM configuration. In these 3D simulations, the dynamics of the gliding arc are computed with the restrike model developed by Bourlet *et al.* [135], as shown in figure 30. The simulations also couple the thermal effects of the gliding arc with combustion kinetics, thus allowing the study of combustion enhancement via thermal, chemical, and turbulent mixing effects.

In addition to the selected results described in this article, it should be noted that the number of publications on scramjet combustion has increased extremely fast in recent years, especially from researchers in China, and it is expected that the field will continue to advance quickly as experimental devices and simulation tools are in place to better understand and optimize these complex systems.

5.2 Detonation-based combustors

An alternative approach to the systems described above is to make use of a supersonic combustion wave, a detonation, described in section 2.1.5 of the companion paper [32]. Extensive research on this process, both fundamental and applied, has been pushed by the development of pressure gain process propulsive systems, such as Pulsed Detonation Engines (PDE) [136], Rotating Detonation Engines (RDE) [137], standing oblique detonation ramjet (SODRAMJET, also known as shock-induced combustion ramjet or SHCRAMJET, not discussed in this review). Furthermore, fundamental understanding of the mechanisms of detonation wave formation are key in risk-mitigation for combustion research and more specifically in the applications listed previously. Knowing fuel-specific values of combustible concentration limits (such as lower explosive and flammability limits), as well as the parameters that lead to or hinder the transition to a detonation (such as temperature and concentration gradients, critical tube dimensions, and critical energy) are important for maintaining safe practices and handling, even in low-pressure, lean, or low-speed studies.

In the spirit of the application-focus of this work, a brief description of the working principle of each system is given. A pulsed detonation engine is a tube with one closed-end filled with a premixed combustible gaseous mixture in which a detonation wave is ignited. As it propagates along the tube, the wave provides thrust. The section is then purged and the cycle repeated at high frequencies. A rotating detonation engine is a cylindrical chamber (or annulus) in which a gaseous combustible mixture is continuously injected. A detonation wave is ignited and rotates azimuthally close to the injection surface, with the hot products ejected and replaced by unburned gases, allowing the detonation to keep propagating and therefore producing thrust. The detailed operating principle of these systems falls outside the scope of this publication and can be found in references [138, 139]. These systems have the benefit of a wide range of efficient velocity operation of the propelled device, from Mach 1.2 to 5, as well as a theoretical increased efficiency with regards to deflagration-based propulsion systems [140]. Unlike the technologies described in the previous section, they can also be comparatively shorter given that compression and combustion both occur through a detonation wave. The integration of these engines into high technological readiness level (TRL) structures requires the consideration of detonation characteristics: materials with high strength to withstand large pressure variations and high temperatures are necessary, and efficient, reliable "at will" ignition under a wide range of conditions is compulsory.

Much like other combustion research, plasmas have been suggested to tackle some of the problems for the operation of these propulsion systems. In this article, two categories using nonequilibrium plasmas will be addressed: (i) Initiating a detonation wave; (ii) Enhancing the propagation of a detonation wave.

5.2.1 Initiation of a detonation wave with nonequilibrium plasma

One of the key study areas in the detonation field is the method of initiation of a detonation wave. Two processes exist: direct initiation or deflagration-to-detonation transition (DDT). In the former, an energy source such as a spark is used to ignite a combustible mixture, depositing sufficient energy that a blast wave is formed and drives a detonation wave. This typically requires large amounts of energy (4 kJ spark in stoichiometric hydrogen-air mixture at 1 bar [141]), unfeasible in practical applications given the requirements for frequent and repeated ignitions. In the latter, a flame is ignited using much lower energies (1 mJ spark in stoichiometric propane-air at 1 bar [142]) and then accelerated through complex multi-physics phenomena, including but not limited to turbulence, pre-compression of the medium ahead of the wave, roughness of the tube in which the flame propagates, concentration and temperature gradients formed by the flame, pressure waves formed by its acceleration, and number of ignition points. Since the start of the XXIst century, multiple authors have suggested the use of various configurations of both nonequilibrium and equilibrium plasmas in order to ignite a detonation wave in a shorter distance and/or shorter time as compared to sparks. Length reduction would allow for smaller propulsive devices, while time reduction would allow for higher operating frequencies. This will be the focus of this section.

Pioneering work in this topic was done by Starikovskiy, Rakitin and Zhukov between 2003 and 2012 [144–148] and is summarized in [149]. Through an extensive series of experiments involving multiple fuels, over a very wide range of pressures (from 150 mbar to 1 bar), they studied the effect of nanosecond plasmas, in single and multi-point ignition, on the reduction of both the DDT time and distance. Their work showed the multiple effects a nonequilibrium plasma could have on the ignition of a detonation wave. They demonstrated shorter DDT lengths and times for a nanosecond multi-point discharge compared to a microsecond spark discharge despite the latter depositing almost 5 times the amount of energy (3 J in the ns, 15 J in the μs) as shown in Figure 32. They also studied different discharge types, namely streamer, transient and spark discharges. Transient and spark discharges were found to lead to fast and short DDT. Streamer discharges enabled the study of

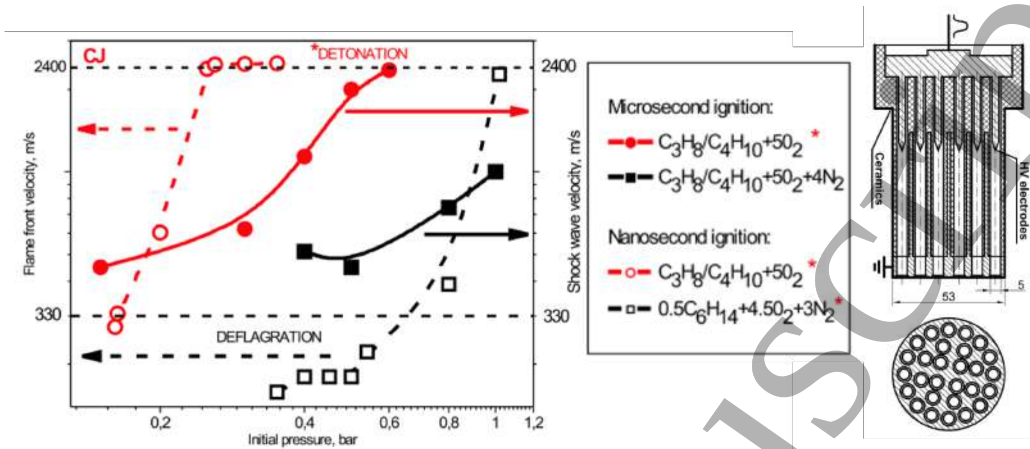

Figure 32: Variations in flame velocity for different pressures and mixtures for nanosecond (full symbols) and microsecond ignition (empty symbols) using the same multi-cell discharge cell (right of the figure). In propane/butane mixture, with (black) and without (red) dilution. Reproduced from Zhukov *et al.* [143].

the gradient mechanism of Zeldovich [150], which led to a DDT with longer time and equivalent length as the other discharge types but with one third of the deposited energy. This mechanism, not to be confused with the Zeldovich mechanism of formation of NO_x discussed earlier in this paper, explains that, in a volume filled with a combustible mixture susceptible to multi-stage ignition, a gradient of parameters can be formed, and ignition will develop according to the gradient mechanism suggested by Zeldovich [150]. In this case, under conditions of non-uniform spatial distribution of temperature/density of chemically active species, a spontaneous combustion wave propagates with a speed determined by the spatial inhomogeneity of the ignition delay time. The speed of such a spontaneous wave can exceed the speed of sound in the medium. A consequence of the development of such a scenario is the rapid formation of shock waves and, in a particular case, detonation waves.

Around the same time, a few other groups were developing ignition methods using nonequilibrium plasma. One such group first presented a Transient Plasma Ignition (TPI) device in the form of a corona discharge designed [151] and tested in conditions closer to real PDE operating conditions as compared to the previous works, performed by Wang [152], Sinibaldi [153], Hutchenson [154], Bubsy [155], Cathey [156] and Singleton [157] *et al.* in the group of Gundersen. The setup, which consisted of an anode rod in a metallic circular tube, was designed such that multiple streamers would be formed and propagate radially. The role of the TPI was evaluated in ground testing PDE facilities for a wide range of conditions, including different fuels (hydrogen, ethylene, propane and aviation gasoline, also known as avgas), equivalence ratios, and mass-flow rates. Results agree that in general, the radial streamers enabled multipoint ignition, leading to fast flames driven by shocks. When compared to spark ignition, for equivalent energy deposition, DDT distance can be reduced by 20% and time by a factor of 2.5, while increasing the ignition probability and extending the operability range.

They pursued more work in transient plasma igniters, such as the one developed by Singleton *et al.* [158, 159]. In their study, they tested two nanosecond discharges: an 85 ns, 90 kV pulse with 800 mJ of deposited energy, referred to as a pseudo-spark and a 12 ns, 60 kV with 180 mJ of deposited energy referred to as a transient plasma igniter. These two igniters were tested in a real PDE configuration (ethylene-air mixture pre-heated to 490 K, 0.35 kg/s mass flow rate, 40 Hz ignition frequency). They varied the equivalence ratio in the range $\phi = 0.6 - 1.2$ and compared the ignition delay time for both discharges. They found minimal differences between the two igniters despite the large disparity in energy deposition, except at lean conditions ($\phi = 0.6$) where the pseudo-spark significantly outperformed the low energy discharge. They attributed the higher energy efficiency of the 12 ns pulse system to a higher estimated volumetric energy. Indeed, due to its smaller size, the 12 ns igniter was estimated to deposit 270 mJ/cm^3, compared to 15 mJ/cm^3. It is important to note that when using a traditional spark, a detonation wave did not occur, hinting that the production of active radicals is likely a key phenomenon.

Leftkowitz *et al.* [44] compared ignition times in a pin-to-pin configuration for a PDE-like setup with varying equivalence ratios of ethylene-air and avgas-air. They tested both an automotive multiple-spark discharge (MSD, 17 mJ across 3 pulses) and NRP discharges (6-64 mJ across a range of pulses at 40 kHz). The deposited energy had no effect on the ignition time and distance in ethylene. In avgas, however, the NRP showed a 25% reduction of ignition time for stoichiometric mixtures at equivalent deposited energies, and a significant extension of the limits of ignition compared to the MSD. It is important to note however that the authors reported no difference in the DDT time, regardless of the conditions tested.

Zheng *et al.* [160–162] similarly looked at ignition of a detonation wave using an AC dielectric-barrier discharge (DBD) compared to a spark discharge for hydrogen-air, acetylene-air, and propane-air mixtures at $\phi = 0.625$. They found that the AC DBD led to a DDT length reduction of 55% for the propane mixture, 60% for the hydrogen mixture and 90% for the acetylene mixture, despite the lower deposited energy in the DBD (0.2 J) compared to the spark (0.5 J). They attributed these results to a faster shock-flame coupling thanks to the enhanced chemical kinetics

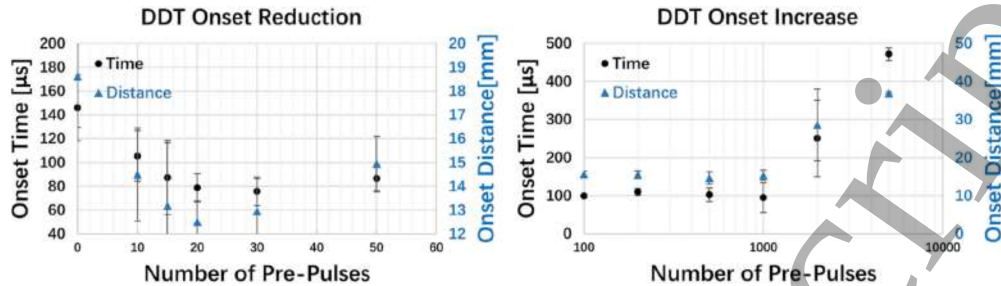

Figure 33: Variations of DDT distance and time with increasing number of applied pulses. Flame ignited by spark. Pre-pulses applied on a 4×500 mm DBD (1 mm gap channel). Reproduced from Vorenkamp *et al.* [166].

caused by the formation of reactive radicals such a O(^{1}D).

The above works studied the formation of a detonation wave ignited by a nonequilibrium plasma and compared it to a thermal spark. Other authors have, however, suggested instead to ignite the mixture with low energy igniters and to use a nonequilibrium plasma to accelerate the DDT. For instance, Gray *et al.* [163, 164] studied the effect of nanosecond plasma in a pulsed 100 kHz pin-to-ring configuration on the flame propagation velocity and DDT length in a hydrogen-air mixture downstream of ignition. Upon ignition with a spark, they found that for 100 applied pulses, the propagation velocity was increased, leading to consistently successful DDT. When the plasma was not applied, DDT never occurred and the flame propagated much slower. This acceleration was explained by a combination of radical production and thermal effect of the plasma as well as shock-flame interaction. They later studied this interaction effect in a set of 8 pin-to-pin electrodes near the wall [165]. Similarly, they found that the pulsed plasma accelerated the flame to transition velocities and much importance was attributed to the shock-flame interaction.

Vorenkamp *et al.* [166, 167] experimentally studied the variation of DDT length and time in a microchannel in a dimethyl ether (DME) oxygen mixture diluted in argon ($\phi = 0.7$). They ignited the mixture with a thermal spark and studied its propagation through a medium which had been conditioned by a plasma formed in a 60 cm long plane-to-plane DBD discharge with varying number of pulses. They were able to reduce the DDT length and time quite significantly by doing this, but this decrease was not proportional to the number of pulses past 30. Indeed, if more pre-pulses were applied, the DDT length and time began to increase again, even increasing past the case where no plasma was applied. This was attributed in part to excessive partial fuel oxidation ahead of the flame, which caused heat release ahead of the flame. Shi et al. [168, 169] ran numerical simulations in a similar geometry for a hydrogen and oxygen mixture and came to similar conclusions about the role of radical production by plasma and its competition with fuel consumption. Further experiments in a similar test-chamber are currently done by Thawko *et al.* [170,171], where the role of ozone is studied for the initiation of a detonation wave based on the gradient mechanism of Zeldovich.

The gradient mechanism of Zeldovich was also studied by Lafaurie *et al.* [172], where a gradient of density of atomic oxygen is generated using nanosecond plasma in order to reduce the DDT distance. O-TALIF measurements confirmed the formation of a gradient of atomic oxygen in air, and its effect on DDT distance and time was studied under action of different gradients [173].

Zhou *et al.* [174, 175] performed several numerical studies in order to show the potential effect of a plane-to-plane AC DBD discharge on DDT acceleration, as well as its relative effect for varying equivalence ratios. Their results show that the addition of the nonequilibrium plasma leads to a reduction of the DDT length and time on the order of 10%, with diminishing efficiency as the equivalence ratio increases past the stoichiometric conditions.

Tropina *et al.* [176, 177] developed a numerical study in which they compared the DDT length and time of a propagating flame which encounters two regions of laser-induced plasma. The comparison was done for a hydrogen-air mixture propagating in a tube with obstacles. After these obstacles, two plasma regions are encountered by the flame. The nonequilibrium plasma was simulated as a source of radicals, while the equilibrium plasma was simulated by Joule heating. The radicals were found to be more efficient at accelerating the flame and therefore decreasing the DDT distance and time than simply heating the gas, although both had an effect.

The plasma-assisted detonation community is uniquely placed to improve the fundamental understanding of deflagration-to-detonation transition as plasma actuation allows for decoupling the complex, multi-physics phenomena initiating DDT. For example, applying plasma to form a gradient of active radicals at ignition allows for the study of gradient mechanisms of Zeldovich. This section has highlighted the many solutions and methods used by different groups over the last two decades, generally aimed at enhancing the DDT efficiency. Efforts have focused on obtaining a shorter transition length or time, with a clear purpose in propulsion applications. Insights gained over the last two decades show the importance of radical production in flame and transition acceleration, either at or downstream from ignition. Flame-shock coupling is a major driver of the transition, and several groups have recently focused on the Zeldovich gradient mechanism to develop "ideal" conditions for the transition. Ultimately, further experimental and numerical research into these topics will benefit both fundamental and applied understanding of the DDT.

5.2.2 Enhancing the detonability of a mixture using nonequilibrium plasma

Reliable ignition of detonations in a short time and distance is not the only technological barrier to overcome in order to implement working detonation engines. The recent increased interest in RDEs culminated in 2021 with the first test flight of a working rotating detonation engine to produce thrust at high altitudes [137]. However, these types of propulsive systems face issues due to their cyclical nature: the detonation wave must propagate in a gas that is not always completely fresh due to the remains of combustion products. In this regard, several solutions have been studied using plasma.

Ali Cherif *et al.* [178, 179] studied the interactions between a detonation wave and a nonequilibrium plasma generated in a plane-to-plane configuration. Testing was done for mixtures of hydrogen-oxygen and methane-oxygen, with and without argon dilution. A nanosecond discharge was applied in the "fresh" gas ahead of a self-sustained detonation wave. When propagating in this region, the detonation dynamics were immediately modified, as the cell size was reduced by a factor of up to two. This was explained by the generation of radicals such as atomic oxygen and atomic hydrogen in the discharge, leading to an increased sensitivity of the fresh mixture to detonation propagation results. Tropina *et al.* [176, 177] obtained similar results in their previously described numerical studies, where the detonation cell size decreased in half with increasing atomic oxygen concentration, due in part to the decrease of the induction length by up to 90%.

Zhu *et al.* [180] implemented a nonequilibrium plasma in a ground testing RDE facility. They compared the reliable operation of the engine for a narrow (4.75 mm) and a wide (27 mm) combustion chamber with and without plasma. Their aim was to enable the propagation of a detonation wave by enhancing the detonability of the mixture from plasma active radical production. For the wide combustion chamber, the effects of the plasma were limited due to difficulty of the discharge to close the gap and the results were complex to interpret because the engine functioned well without the addition of radicals. In the narrow chamber without plasma, they observed a brief period of unstable detonation for an equivalence ratio of $\phi = 1.2$. Upon igniting the 3 kHz, 40 kV nanosecond plasma, they were able to extend the range of unstable detonation for equivalence ratios $\phi = 1 - 1.4$ and observed several detonation reignition events. They explained these results with plasma kinetic modeling and a Zeldovich Neumann Döring (ZND) detonation model showing that the plasma led to significant cell size reduction and therefore increased detonability.

Although fewer studies exist on detonability enhancement, all results seem to point towards a demonstrable effect of nonequilibrium plasma to enhance the range of propagation of a self-sustained detonation wave due to the formation of radicals. This is a promising result for the field of propulsion, specifically to overcome potential issues in rotating detonation engines.

In brief conclusion, the field of plasma-assisted detonation, while still emergent, already seems to offer some solutions to practical challenges posed by supersonic combustion. Further research is necessary into the fundamental aspects of DTT, hopefully enabling, a more complete understanding of the mechanisms leading to detonation formation. This could be achieved by specifically acting on a subset of the possible phenomena, for example, gradients of concentration, leading to safer practices and new technology development.

6 Conclusions and recommendations for future research

Intense research on plasma-assisted combustion for the past two decades has brought a wealth of fundamental results to understand the thermal, chemical and transport effects of plasmas in flames. Nonequilibrium plasma have been shown to be an effective method to promote lean flame stabilization, extend operability limits, mitigate thermo-acoustic instabilities, and enhance supersonic combustion. They were also shown to be energy efficient, as the required electrical power is typically between 0.001% and 1% of the flame thermal power. The systems used to produce these plasma are typically based on solid state technologies that have the advantages of being compact, lightweight, and power efficient. Remarkable progress has also been accomplished in the past few years regarding numerical simulations of plasma-assisted combustion. The effects induced by nonequilibrium discharges can now be incorporated into the conventional computational fluid dynamics tools of the combustion community, opening the way to representative simulations for the design and optimization of plasma systems under a wide range of conditions. As a result, these advances have attracted strong interest from the combustion community who is currently applying nonequilibrium plasmas to various innovative staged combustion systems representative of aircraft and power generation gas turbines to decrease NO_x emissions, improve performance, and increase fuel flexibility. Promising results were also obtained for the enhancement of combustion in supersonic and detonation-based engines.

Several challenges remain at this stage. First, the demonstration experiments have been limited to pressures below 7 bars and flame powers below a few 100 kW. However, the pressure in gas turbines can be much higher, as high pressures increase the combustion outlet temperature and thus the conversion efficiency. Current jet engines operate at pressures up to 40 bars and powers on the order of 10 MW, and for stationary gas turbines the pressure and power can be up to 30 bars and 600 MW, respectively. As the pressure increases, electrical breakdown becomes more difficult. In a 2000 K combustor at 40 bars, for example, the breakdown voltage across a 5 mm gap is around 80 kV. These high voltages require careful handling and may pose electromagnetic interference issues. Adjustments may be necessary to reduce the inter-electrode distance or to apply different voltage excitation patterns to ensure efficient and safe operation under these high-pressure conditions. In addition, high pressures are also associated with higher gas densities, which may have an impact on the effectiveness of the plasma because of changes in the frequency of collisions. In particular, nonequilibrium conditions are more difficult to sustain at high pressure because three-body reactions are enhanced, and the plasma diameter and uniformity decrease. Higher flame powers also mean that higher discharge powers are required. Thus, additional efforts should be pursued to examine novel discharge types and pulsing patterns to continue reducing the required plasma power.

Second, another challenge is to gain a better understanding of the formation mechanisms of pollutants, particularly NO_x, in plasma-assisted flames. Further work is required to determine the discharge conditions that will allow sufficient radicals production while minimizing the formation of NO_x and other pollutants.

Third, extension to flames with synthetic fuels, hydrogen, ammonia, and mixtures of these fuels with conventional fossil fuels is becoming of increasing interest. Combustion of these fuels faces similar challenges in terms of LBO and TAI as traditional fossil fuels. Although several experimental studies have shown that PAC is also highly effective for these fuels, there are still several issues to examine, notably the ability to control flashback with the highly reactive hydrogen flames, or to reduce NO_x in ammonia flames.

Fourth, active control strategies for the reduction of thermo-acoustic instabilities must still be implemented. To this end, it is required to better understand the inter-coupling between the flame, the flow and the plasma to incorporate in existing TAI models the various discharge parameters such as plasma power, PRF, and reduced electric field.

Fifth, demonstrations in more realistic environments, such as an annular combustor or a can-combustor with high Reynolds number, multiple flames, and azimuthal acoustic modes are still missing.

Finally, the integration of plasma systems requires more detailed investigations. PAC systems using the electrodes already in place for device ignition, with minor modifications, would be the ideal option to ensure drop-in solutions. However, these

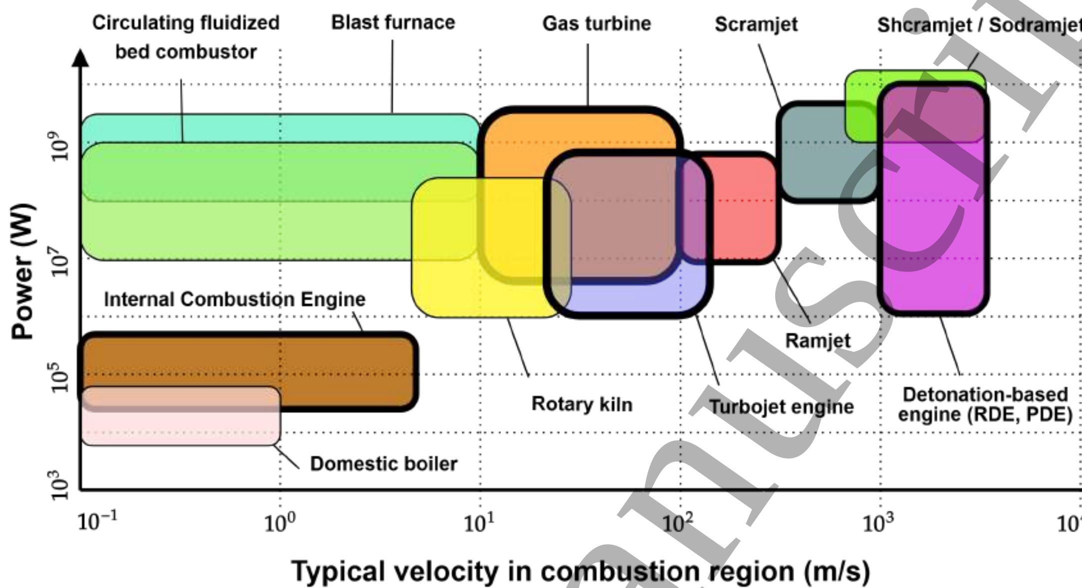

Figure 34: Typical powers and flow velocities in combustion applications. The orders of magnitude are indicative. Bold frames indicate applications for which PAC is currently being investigated. Future potential areas of interest include include industrial kilns and furnaces.

electrodes are often placed near the combustion chamber wall, which may not be the most effective location for PAC. Thus further work is needed to ensure effective combustion enhancement while minimizing modifications to the chamber.

Plasma-assisted combustion shows great promise as a flexible, versatile, energy-efficient technology to answer the issues of combustion systems with both traditional and novel fuels. In addition to the power production and transportation applications covered in this article, there are many other areas where PAC could potentially bring solutions. These include notably industrial furnaces for chemical and material processing as generally indicated in figure 34.

Acknowledgments

The work of J.-B. P.-T. and C.O.L was supported by the European Research Council (ERC) under the GreenBlue project of the European Union's Horizon 2020 research and innovation programme (grant agreement No. 101021538).

The work of S.M.S. was partially supported by the European Union project CAIPIRINH3A under grant agreement No. 101191768. The work of V.L. and S.M.S. was also partially supported by Agence de l'Innovation de Défense – AID - via Centre Interdisciplinaire d'Etudes pour la Défense et la Sécurité – CIEDS - (project 2022 - PPRINCE) and Energy4Climate Interdisciplinary Center (E4C) of IP Paris and Ecole des Ponts - ParisTech in the framework of the 3rd Programme d'Investissements d'Avenir, ANR-18-EUR-0006-02. Views and opinions expressed are however those of the authors only and do not necessarily reflect those of the European Union or CINEA.

The authors would like to thank Dr. Pierre Vidal, Dr. Alexander Konnov, Dr. Nikolay Aleksandrov, Dr. Nikolay Popov, Dr. Alejandro Alvarez, Dr. Daniel Durox, Dr. Sébastien Ducruix, Stéphane Wang and Nicolas Vaysse for numerous discussions, valuable critiques, insightful proofreading, and constructive advice. The authors express their sincere gratitude to their colleagues and students for the privilege of working with them and for the inspiration they have provided over years and decades of research.

Appendix: Nomenclature of NRP discharge regimes

NRP discharges can produce different plasma regimes, depending on the applied voltage, pulse duration, energy per pulse, and initial gas temperature and composition. As their nomenclature can be confusing to readers not familiar with the field, we provide here a short summary of the various types mentioned in the NRP literature.

Streamer (or ionization wave, or corona): For a comprehensive discussion of streamer physics and characteristics, the reader is referred to the tutorial review of Nijdam *et al.* [181]. Basically, all discharges initiate with an electrode avalanche, which corresponds to the multiplication of electrons under ionizing collisions. When the electron number density reaches a critical value (Meek-Loeb criterion), the head and tail of the avalanche start propagating much faster under the enhanced local field created by space charges. A streamer is created. Typical electron number densities in the streamer head are on the order of 10^{13}-10^{15} cm^{-3}. The degree of gas heating is typically low ($<$ 200 K). The speed of propagation of streamers depends on the electric field and the gas, with typical values on the order of 1 mm/ns. If the streamer fades before reaching the opposite electrode, the discharge takes the form of a corona, with localized emission around the electrode. If the electric field is maintained past the moment that the streamer has traversed the interelectrode gap (for a 10-ns pulse applied in air in a 5 mm gap at atmospheric pressure, the streamer will cross the gap in 5 ns, and the voltage continues to be applied for another 5 ns), the plasma parameters become uniform across the gap and the discharge transforms into a glow or a spark. These regimes are described next.

Glow discharge: Once the streamer has crossed the gap, conduction current flows through the discharge. The channel undergoes Joule heating and thermal diffusion cooling. If the latter dominates, the gas temperature does not increase significantly (typically $<$ 200 K), the electron number density stays below 10^{15} cm^{-3}. The conduction current is typically $<$ 1 A and the deposited electric energy is typically $<$ 100 µJ. This regime is often referred to as an NRP glow discharge, by analogy to DC glow discharges [182].

Spark: Above a certain pulse energy, Joule heating may dominate over diffusive cooling of the channel after the streamer has crossed the gap. In air, the gas temperature increases significantly ($>$ 1000 K) and the electron density reaches values between 10^{15} cm^{-3} and full ionization. Typical conduction currents are $>$ 10 A and the deposited energy is on the order of mJ. Three types of spark discharges can be encountered:

Non-thermal spark: This is the case if the gas temperature increase ($\sim$ 1000 K) remains much below the electron temperature. Ionization increases to 10^{15}-10^{17} cm^{-3} and significant molecular dissociation occurs. Typical examples are described in [34,37]. In air, the diameter of the non-thermal spark is $\sim$ 1 mm. The plasma is in a state of both thermal and chemical nonequilibrium, hence the name nonequilibrium spark.

Thermal spark: If sufficient ionization is created along the centerline of the discharge axis (or near the electrodes), a narrow strongly ionized filament (~ 100 µm in diameter) appears on the axis of the discharge, as observed by [183–191]. Owing to the high frequency of electron-ion collisions, the gas and electron temperatures equalize during the pulse at high values on the order of 20,000 – 60,000 K. Because the equality of T_e and T_g corresponds to the definition of a thermal plasma, the term of thermal spark was introduced in [191] to characterize this nanosecond spark regime. It should be noted however that the plasma is not necessarily in chemical equilibrium. The kinetic mechanism describing the transition to the thermal spark was shown to be caused by multi-step ionization kinetics of atomic and molecular species [192] and was numerically simulated in 2D by Zhang *et al.* [193].

LTE spark: If the pulse duration is longer than the characteristic time of chemical reactions, the plasma can reach chemical equilibrium in addition to thermal equilibrium during the pulse. The combination of thermal and chemical equilibrium corresponds to Local Thermodynamic Equilibrium. Hence the name LTE spark. The LTE spark was evidenced by Maillard *et al.* [194], who also characterized non-thermal, thermal and LTE sparks in a CO_2 discharge. They showed that the diameter of the thermal and LTE sparks are on the order of 100 µm, and that they are simultaneously surrounded by a wider non-thermal region of diameter around 1 mm.

The frontier between the glow and spark regimes is usually clearly seen as it is accompanied by an abrupt and strong increase in light emission and deposited energy. On the other hand, the frontier between the nonequilibrium and the thermal/LTE spark is not easily observed visually, and there is practically no change in deposited energy at the limits between the nonequilibrium, thermal, and LTE discharges. The conduction current is practically the same in all three cases: however, the current density in the narrow channel of LTE/thermal sparks is much higher than in the wider channel of nonequilibrium sparks. To distinguish these regimes, it is often necessary to resort to optical measurements of electron number density. In air, several emission features can be used to distinguish between these regimes: N_2 second positive emission is clearly seen in nonequilibrium sparks but not in thermal/LTE sparks, whereas the latter discharges feature prominent lines of atomic ions. Finally, it should be noted that the thermal and LTE spark channels are surrounded by a nonthermal spark channel [194]. Beyond their impact on the thermochemical state of the plasma, the various plasma regimes also influence flow dynamics with the creation of shock waves and flow recirculation regions in the post-discharge. For pin-to-pin NRP discharges, Roger *et al.* [195] provided a simple criterion; they showed that recirculation occurs when the temperature of the plasma at the end of the pulse is about 10 times higher than the temperature of the ambient gases surrounding the plasma kernel ($T_{plasma}/T_{ambient} > 10$).

Table 3 provides estimates of the plasma properties in the various regimes, based on the aforementioned observations in ambient or preheated air and CO_2 at atmospheric pressure.

Table 3: Charateristics of NRP regimes in ambient gases between pin-pin electrodes (the limits are indicative and should not be taken too strictly).

Regime name	Energy	Diameter	Gas heating ($+\Delta T_{gas}$)	Electron number density (cm^{-3})	Conduction current
Corona	$< 1\mu J$	–	< 200 K	$\sim 10^{13} - 10^{15}$	< 1 A
Glow	$< 100\ \mu J$	–	< 200 K	$\sim 10^{13} - 10^{15}$	< 1 A
Nonequilibrium Spark	∼mJ	∼1 mm	∼1000 K	$\sim 10^{15} - 10^{17}$	$\sim 10 - 100$ A
Thermal spark	∼mJ	$\sim 100\ \mu m$	$20 - 60$kK	$\sim 10^{19}$ (fully ionized)	$\sim 1 - 100$ A
LTE spark	∼mJ	$\sim 100\ \mu m$	$20 - 60$kK	$\sim 10^{19}$ (fully ionized)	$\sim 10 - 100$ A

References

[1] Lefebvre A H and Ballal D R 2010 *Gas Turbine Combustion: Alternative Fuels and Emissions* 3rd ed (Boca Raton: CRC Press) ISBN 978-0-429-14104-1

[2] Liu Y, Sun X, Sethi V, Nalianda D, Li Y G and Wang L 2017 Review of Modern Low Emissions Combustion Technologies for Aero Gas Turbine Engines *Progress in Aerospace Sciences* **94** 12–45

[3] Huang Y and Yang V 2009 Dynamics and Stability of Lean-Premixed Swirl-Stabilized Combustion *Prog. Energy Combust. Sci.* **35** 293–364

[4] Candel S 2002 Combustion Dynamics and Control: Progress and Challenges *Proc. Combust. Inst.* **29** 1–28

[5] Ju Y and Sun W 2015 Plasma Assisted Combustion: Dynamics and Chemistry *Progress in Energy and Combustion Science* **48** 21–83

[6] Starikovskiy A Yu and Aleksandrov N 2013 Plasma-Assisted Ignition and Combustion *Progress in Energy and Combustion Science* **39** 61–110

[7] Starikovskaia S M 2006 Plasma Assisted Ignition and Combustion *J. Phys. D: Appl. Phys.* **39** R265–R299

[8] Ju Y, Mao X, Lefkowitz J K and Zhong H 2023 Plasma-Assisted Hydrogen Combustion *Hydrogen for Future Thermal Engines* Green Energy and Technology ed Tingas E A (Springer Nature Switzerland AG)

[9] Kruger C H, Laux C O, Yu L, Packan D M and Pierrot L 2002 Nonequilibrium Discharges in Air and Nitrogen Plasmas at Atmospheric Pressure *Pure Appl. Chem.* **74** 337–347

[10] Pilla G, Galley D, Lacoste D A, Lacas F, Veynante D and Laux C 2006 Stabilization of a Turbulent Premixed Flame Using a Nanosecond Repetitively Pulsed Plasma *IEEE Trans. Plasma Sci.* **34** 2471–2477

[11] Kim W, Godfrey Mungal M and Cappelli M A 2010 The Role of in Situ Reforming in Plasma Enhanced Ultra Lean Premixed Methane/Air Flames *Combust. Flame* **157** 374–383

[12] Pham Q L L, Lacoste D A and Laux C O 2011 Stabilization of a Premixed Methane–Air Flame Using Nanosecond Repetitively Pulsed Discharges *IEEE Trans. Plasma Sci.* **39** 2264–2265

[13] Barbosa S, Pilla G, Lacoste D A, Scouflaire P, Ducruix S, Laux C O and Veynante D 2015 Influence of Nanosecond Repetitively Pulsed Discharges on the Stability of a Swirled Propane/Air Burner Representative of an Aeronautical Combustor *Phil. Trans. R. Soc. A.* **373** 20140335

[14] Gomez Del Campo F, Weibel D E and Wen C 2017 Preliminary Results from a Plasma-Assisted 7-Point Lean Direct Injection (LDI) Combustor and Resulting Impacts on Combustor Stability and Combustion Dynamics *53rd AIAA SAE ASEE Jt. Propuls. Conf.* (AIAA) 2017-4778

[15] Heid G, Pilla G, Lecourt R and Lacoste D A 2009 Assisted Combustion Of An Air Kerosene Mixture By Nanosecond Repetitively Pulsed Discharges *International Symposium on Air Breathing Engines ;* (AIAA) 474-482

[16] Di Sabatino F and Lacoste D A 2020 Enhancement of the Lean Stability and Blow-off Limits of Methane-Air Swirl Flames at Elevated Pressures by Nanosecond Repetitively Pulsed Discharges *J. Phys. D: Appl. Phys.* **53** 355201

[17] Vignat G, Minesi N, Soundararajan P R, Durox D, Renaud A, Blanchard V, Laux C O and Candel S 2021 Improvement of Lean Blow out Performance of Spray and Premixed Swirled Flames Using Nanosecond Repetitively Pulsed Discharges *Proc. Combust. Inst.* **38** 6559–6566

[18] Choe J, Sun W, Ombrello T and Carter C 2021 Plasma Assisted Ammonia Combustion: Simultaneous NOx Reduction and Flame Enhancement *Combust. Flame* **228** 430–432

[19] Blanchard V P, Scouflaire P, Laux C O and Ducruix S 2023 Combustion Performance of Plasma-Stabilized Lean Flames in a Gas Turbine Model Combustor *Applications in Energy and Combustion Science* **15** 100158

[20] Aravind B, Yu L and Lacoste D 2023 Enhancement of Lean Blowout Limits of Swirl Stabilized NH3-CH4-Air Flames Using Nanosecond Repetitively Pulsed Discharges at Elevated Pressures *Applications in Energy and Combustion Science* **16** 100225

[21] Perrin-Terrin J B, Vaysse N, Durox D, Vicquelin R, Candel S, Laux C O and Renaud A 2024 Plasma-Assisted Combustion of Hydrogen Swirling Flames: Extension of Lean Blowout Limit and NOx Emissions *Proc. Combust. Inst.* **40** 105546

[22] Shanbhogue S, Dijoud R, Pavan C, Rao S R, Gomez del Campo F, Guerra-Garcia C and Ghoniem A 2024 Emissions and Dynamic Stability Improvements in Premixed CH_4/NH_3 Swirling Flames with Nanosecond Pulsed Plasmas *AIAA Aviation Forum and ASCEND Conference* 2024-3898

[23] Kim G T, Yoo C S, Chung S H and Park J 2020 Effects of Non-Thermal Plasma on the Lean Blowout Limits and CO/NOx Emissions in Swirl-Stabilized Turbulent Lean-Premixed Flames of Methane/Air *Combust. Flame* **212** 403–414

[24] Michael J B, Chng T L and Miles R B 2013 Sustained Propagation of Ultra-Lean Methane/Air Flames with Pulsed Microwave Energy Deposition *Combust. Flame* **160** 796–807

[25] Matveev I, Matveeva S, Kirchuk E and Serbin S 2008 Experimental and Theoretical Investigations of a Triple Vortex Combustor with Spatial Arc *46th AIAA Aerosp. Sci. Meet. Exhib.* (AIAA) 2008-963

[26] Liu X, Ahamed Subash A, Bao Y, Li Z, Ehn A, Hurtig T, Larfeldt J, Lörstad D, Nilsson T and Fureby C 2022 Plasma Effects on Swirl Flames in a Scaled Dry Low Emission Burner *AIAA Journal* **60** 3813–3820

[27] Tang Y, Sun J, Shi B, Li S and Yao Q 2021 Extension of Flammability and Stability Limits of Swirling Premixed Flames by AC Powered Gliding Arc Discharges *Combust. Flame* **231** 111483

[28] Sun J, Tang Y and Li S 2021 Plasma-Assisted Stabilization of Premixed Swirl Flames by Gliding Arc Discharges *Proc. Combust. Inst.* **38** 6733–6741

[29] Liu Q, Baccarella D and Lee T 2020 Review of Combustion Stabilization for Hypersonic Airbreathing Propulsion *Progress in Aerospace Sciences* **119** 100636

[30] Blanchard V 2023 *Thermochemical Effects of Nanosecond Plasma Discharges on Lean Flame Stabilization* Ph.D. thesis Université Paris-Saclay

[31] Lin B, Wu Y, Zhu Y, Song F and Bian D 2019 Experimental Investigation of Gliding Arc Plasma Fuel Injector for Ignition and Extinction Performance Improvement *Applied Energy* **235** 1017–1026

[32] Starikovskaia S M, Lafaurie V, Perrin-Terrin J B and Laux C O 2025 Foundations of Plasma-Assisted Combustion. Part 1: Fundamentals of Combustion and Plasma. *Plasma Sources Sci. T.* **(in process)**

[33] Popov N A 2001 Investigation of the Mechanism for Rapid Heating of Nitrogen and Air in Gas Discharges *Plasma Phys. Rep.* **27** 886–896

[34] Pai D Z, Lacoste D A and Laux C O 2010 Nanosecond Repetitively Pulsed Discharges in Air at Atmospheric Pressure—the Spark Regime *Plasma Sources Sci. Technol.* **19** 065015

[35] Stancu G D, Janda M, Kaddouri F, Lacoste D A and Laux C O 2010 Time-Resolved CRDS Measurements of the N_2 ($A^3\Sigma_u{}^+$) Density Produced by Nanosecond Discharges in Atmospheric Pressure Nitrogen and Air *J. Phys. Chem. A* **114** 201–208

[36] Mintoussov E I, Pendleton S J, Gerbault F G, Popov NA and Starikovskaia SM 2011 Fast Gas Heating in Nitrogen–Oxygen Discharge Plasma: II. Energy Exchange in the Afterglow of a Volume Nanosecond Discharge at Moderate Pressures *J. Phys. Appl. Phys.* **44** 285202

[37] Rusterholtz D L, Lacoste D A, Stancu G D, Pai D Z and Laux C O 2013 Ultrafast Heating and Oxygen Dissociation in Atmospheric Pressure Air by Nanosecond Repetitively Pulsed Discharges *J. Phys. D: Appl. Phys.* **46** 464010

[38] Lo A, Cessou A, Boubert P and Vervisch P 2014 Space and Time Analysis of the Nanosecond Scale Discharges in Atmospheric Pressure Air: I. Gas Temperature and Vibrational Distribution Function of N2 and O2 *J. Phys. D: Appl. Phys.* **47** 115201

[39] Lo A, Cessou A and Vervisch P 2014 Space and Time Analysis of the Nanosecond Scale Discharges in Atmospheric Pressure Air: II. Energy Transfers during the Post-Discharge *J. Phys. D: Appl. Phys.* **47** 115202

[40] Xu D, Lacoste D A and Laux C O 2013 Temporal and Spatial Evolution of OH Concentration in a Lean Premixed Propane-Air Flame Assisted by Nanosecond Repetitively Pulsed Discharges *51st AIAA Aerosp. Sci. Meet. New Horiz. Forum Aerosp. Expo.* (AIAA) 2013-895

[41] Xu D A 2013 *Thermal and Hydrodynamic Effects of Nanosecond Discharges in Air and Application to Plasma-Assisted Combustion* Ph.D. thesis Ecole Centrale Paris

[42] Pilla G 2008 *Etude Expérimentale de La Stabilisation de Flammes Propane-Air de Prémélange Par Décharges Nanosecondes Impulsionnelles Répétitives* Ph.D. thesis Ecole Centrale Paris

[43] Adamovich I V, Li T and Lempert W R 2015 Kinetic Mechanism of Molecular Energy Transfer and Chemical Reactions in Low-Temperature Air-Fuel Plasmas *Philos. Trans. R. Soc. Math. Phys. Eng. Sci.* **373** 20140336

[44] Lefkowitz J K, Guo P, Ombrello T, Won S H, Stevens C A, Hoke J L, Schauer F and Ju Y 2015 Schlieren Imaging and Pulsed Detonation Engine Testing of Ignition by a Nanosecond Repetitively Pulsed Discharge *Combust. Flame* **162** 2496–2507

[45] DeFilippo A C and Chen J Y 2016 Modeling Plasma-Assisted Methane–Air Ignition Using Pre-Calculated Electron Impact Reaction Rates *Combust. Flame* **172** 38–48

[46] Popov N A 2016 Kinetics of Plasma-Assisted Combustion: Effect of Non-Equilibrium Excitation on the Ignition and Oxidation of Combustible Mixtures *Plasma Sources Sci. Technol.* **25** 043002

[47] Deak N, Bellemans A and Bisetti F 2021 Plasma-Assisted Ignition of Methane/Air and Ethylene/Air Mixtures: Efficiency at Low and High Pressures *Proc. Combust. Inst.* **38** 6551–6558

[48] Bellemans A, Kincaid N, Deak N, Pepiot P and Bisetti F 2021 P-DRGEP: A Novel Methodology for the Reduction of Kinetics Mechanisms for Plasma-Assisted Combustion Applications *Proc. Combust. Inst.* **38** 6631–6639

[49] Bellemans A, Deak N and Bisetti F 2020 Development of Skeletal Kinetics Mechanisms for Plasma-Assisted Combustion via Principal Component Analysis *Plasma Sources Sci. Technol.* **29** 025020

[50] Cheng L, Barleon N, Cuenot B, Vermorel O and Bourdon A 2022 Plasma Assisted Combustion of Methane-Air Mixtures: Validation and Reduction *Combust. Flame* **240** 111990

[51] Pavan C A 2023 *Nanosecond Pulsed Plasmas in Dynamic Combustion Environments* Ph.D. thesis Massachusetts Institute of Technology

[52] Bak M S, Do H, Mungal M G and Cappelli M A 2012 Plasma-Assisted Stabilization of Laminar Premixed Methane/Air Flames around the Lean Flammability Limit *Combust. Flame* **159** 3128–3137

[53] Yin Z, Adamovich I V and Lempert W R 2013 OH Radical and Temperature Measurements during Ignition of H2-air Mixtures Excited by a Repetitively Pulsed Nanosecond Discharge *Proc. Combust. Inst.* **34** 3249–3258

[54] Tholin F and Bourdon A 2014 Influence of the External Electrical Circuit on the Regimes of a Nanosecond Repetitively Pulsed Discharge in Air at Atmospheric Pressure *Plasma Phys. Control. Fusion* **57** 014016

[55] Sharma A, Subramaniam V, Solmaz E and Raja L L 2018 Fully Coupled Modeling of Nanosecond Pulsed Plasma Assisted Combustion Ignition *J. Phys. D: Appl. Phys.* **52** 095204

[56] Pavan C A and Guerra-Garcia C 2023 Modeling Flame Speed Modification by Nanosecond Pulsed Discharges to Inform Experimental Design *AIAA Scitech 2023 Forum* (AIAA) 2023-2056

[57] Castela M, Fiorina B, Coussement A, Gicquel O, Darabiha N and Laux C O 2016 Modelling the Impact of Non-Equilibrium Discharges on Reactive Mixtures for Simulations of Plasma-Assisted Ignition in Turbulent Flows *Combust. Flame* **166** 133–147

[58] Bechane Y and Fiorina B 2021 Numerical Investigations of Turbulent Premixed Flame Ignition by a Series of Nanosecond Repetitively Pulsed Discharges *Proc. Combust. Inst.* **38** 6575–6582

[59] Blanchard V P, Bechane Y, Minesi N Q, Wang S Q E, Fiorina B and Laux C O 2024 Experimental Characterization and 3D Simulations of Turbulent Flames Assisted by Nanosecond Plasma Discharges *Combust. Flame* **270** 113709

[60] Poinsot T and Veynante D 2005 *Theoretical and Numerical Combustion* (R.T. Edwards, Inc.) ISBN 978-1-930217-10-2

[61] Malé Q, Shcherbanev S and Noiray N 2023 Numerical Study of Plasma Assisted Combustion in a Sequential Combustor *Proc. Combust. Inst.* **39** 5447–5456

[62] Barléon N, Cheng L, Cuenot B and Vermorel O 2023 A Phenomenological Model for Plasma-Assisted Combustion with NRP Discharges in Methane-Air Mixtures: PACMIND *Combust. Flame* **253** 112794

[63] Shao X, Lacoste D A and Im H G 2024 A Computational Study of Plasma-Assisted Ammonia/Hydrogen Combustion Using a Phenomenological Model *AIAA Scitech 2024 Forum* (AIAA) 2024-0598

[64] Taneja T S, Ombrello T, Lefkowitz J and Yang S 2024 Large Eddy Simulation of Plasma Assisted Ignition: Effects of Pulse Repetition Frequency, Number of Pulses, and Pulse Energy *Combust. Flame* **267** 113574

[65] Wang S Q E, Bechane Y, Darabiha N and Fiorina B 2023 Efficiency Analysis of Ignition by Nanosecond Repetitively Pulsed Discharges Using a Low-Order Model *Applications in Energy and Combustion Science* **15** 100166

[66] Kruljevic B, Wand S Q E, Vaysse N, Perrin-Terrin J B, Durox D, Renaud A, Laux C O and Fiorina B 2025 Numerical Study on the Impact of Nanosecond Repetitively Pulsed Discharges on the Lean Blowout Limit for a Hydrogen/Air Swirled Flame *Combust. Flame* **277** 114149

[67] Malé Q, Barléon N, Shcherbanev S, Dharmaputra B and Noiray N 2024 Numerical Study of Nitrogen Oxides Chemistry during Plasma Assisted Combustion in a Sequential Combustor *Combust. Flame* **260** 113206

[68] Malé Q, Shcherbanev S, Impagnatiello M and Noiray N 2024 Stabilization of a Thermoacoustically Unstable Sequential Combustor Using Non-Equilibrium Plasma: Large Eddy Simulation and Experiments *Proc. Combust. Inst.* **40** 105277

[69] Alkhalifa A M, Sabatino F Di, Steinmetz S A, Pfaff S, Huang E, Frank J H, Kliewer C J and Lacoste D A 2024 Quantifying the Thermal Effect and Methyl Radical Production in Nanosecond Repetitively Pulsed Glow Discharges Applied to a Methane-Air Flame *J. Phys. D: Appl. Phys.* **57** 385204

[70] Güthe F, Hellat J and Flohr P 2009 The Reheat Concept: The Proven Pathway to Ultralow Emissions and High Efficiency and Flexibility *J. Eng. Gas Turbines Power* **131** 021503

[71] Mongia H and Dodds W 2004 Low Emissions Propulsion Engine Combustor Technology Evolution Past, Present and Future *24th Congress of International Council of the Aeronautical Sciences* (Yokohama, Japan)

[72] Truffot M, Renaud A, Zimmer L, Richecoeur F, Cayre A and Méry Y 2023 Intermittency of Flame Structure and Thermo-Acoustic Behavior in a Staged Multipoint Injector Using Liquid Fuel *ASME Turbo Expo 2023: Turbomachinery Technical Conference and Exposition* (American Society of Mechanical Engineers Digital Collection)

[73] Mesquita L C C, Vié A, Zimmer L and Ducruix S 2021 Numerical Analysis of Flame Shape Bifurcation in a Two-Stage Swirled Liquid Burner Using Large Eddy Simulation *Proc. Combust. Inst.* **38** 5971–5978

[74] Lucca-Negro O and O'Doherty T 2001 Vortex Breakdown: A Review *Progress in Energy and Combustion Science* **27** 431–481

[75] Cunha Caldeira Mesquita L 2021 *Simulation and Analysis of the Shape, Performance and Stability of Flames in a Two-Stage Lean-Burn Aeronautical Combustor* Ph.D. thesis Université Paris-Saclay

[76] Lieuwen T C and Yang V 2005 *Combustion Instabilities In Gas Turbine Engines: Operational Experience, Fundamental Mechanisms, and Modeling* (AIAA) ISBN 978-1-56347-669-3 978-1-60086-680-7

[77] Poinsot T 2017 Prediction and Control of Combustion Instabilities in Real Engines *Proc. Combust. Inst.* **36** 1–28

[78] Schuller T, Poinsot T and Candel S 2020 Dynamics and Control of Premixed Combustion Systems Based on Flame Transfer and Describing Functions *J. Fluid Mech.* **894** P1

[79] Rayleigh 1878 The Explanation of Certain Acoustical Phenomena 1 *Nature* **18** 319–321

[80] Durox D, Schuller T, Noiray N, Birbaud A L and Candel S 2009 Rayleigh Criterion and Acoustic Energy Balance in Unconfined Self-Sustained Oscillating Flames *Combust. Flame* **156** 106–119

[81] Dharmaputra B, Shcherbanev S, Schuermans B and Noiray N 2023 Thermoacoustic Stabilization of a Sequential Combustor with Ultra-Low-Power Nanosecond Repetitively Pulsed Discharges *Combust. Flame* **258** 113101

[82] Noiray N, Durox D, Schuller T and Candel S 2008 A Unified Framework for Nonlinear Combustion Instability Analysis Based on the Flame Describing Function *J. Fluid Mech.* **615** 139–167

[83] Paschereit C O, Schuermans B, Polifke W and Mattson O 2002 Measurement of Transfer Matrices and Source Terms of Premixed Flames *J. Eng. Gas Turbines Power* **124** 239–247

[84] Lacoste D A, Moeck J P, Paschereit C O and Laux C O 2013 Effect of Plasma Discharges on Nitric Oxide Emissions in a Premixed Flame *J. Propuls. Power* **29** 748–751

[85] Moeck J, Lacoste D A, Laux C O and Paschereit C 2013 Control of Combustion Dynamics in a Swirl-Stabilized Combustor with Nanosecond Repetitively Pulsed Discharges *51st AIAA Aerosp. Sci. Meet. New Horiz. Forum Aerosp. Expo.* 2013-565

[86] Alkhalifa A M, Alsalem A, Del Cont-Bernard D and Lacoste D A 2023 Active Control of Thermoacoustic Fluctuations by Nanosecond Repetitively Pulsed Glow Discharges *Proc. Combust. Inst.* **39** 5429–5437

[87] Di Sabatino F, Guiberti T F, Moeck J P, Roberts W L and Lacoste D A 2021 Actuation Efficiency of Nanosecond Repetitively Pulsed Discharges for Plasma-Assisted Swirl Flames at Pressures up to 3 Bar *J. Phys. D: Appl. Phys.* **54** 075208

[88] Yu L, Aravind B and Lacoste D A 2023 Mitigating the Response of Premixed Swirl Flames to Acoustic Excitation by Nanosecond Repetitively Pulsed Discharges at Elevated Pressures *Combust. Flame* **256** 112944

[89] Kim W and Cohen J 2021 Plasma-Assisted Combustor Dynamics Control at Realistic Gas Turbine Conditions *Combust. Sci. Technol.* **193** 869–888

[90] Kim W, Snyder J and Cohen J 2015 Plasma Assisted Combustor Dynamics Control *Proc. Combust. Inst.* **35** 3479–3486

[91] Shanbhogue S J, Pavan C A, Weibel D E, Gomez Del Campo F, Guerra-Garcia C and Ghoniem A F 2023 Control of Large-Amplitude Combustion Oscillations Using Nanosecond Repetitively Pulsed Plasmas *J. Propuls. Power* **39** 469–481

[92] Pavan C A, Shanbhogue S J, Weibel D E, Gomez Del Campo F, Ghoniem A F and Guerra-Garcia C 2024 Dynamic Response of Nanosecond Repetitively Pulsed Discharges to Combustion Dynamics: Regime Transitions Driven by Flame Oscillations *Plasma Sources Sci. Technol.* **33** 025016

[93] Dharmaputra B, Shcherbanev S and Noiray N 2024 Plasma Assisted Thermoacoustic Stabilization of a Transiently Operated Sequential Combustor at High Pressure *Proc. Combust. Inst.* **40** 105518

[94] Aravind B, Yu L and Lacoste D A 2024 Understanding the Coupling between Nanosecond Repetitively Pulsed Discharges and the Thermoacoustic Behavior of a Swirl Flame at 2 Bar *Proc. Combust. Inst.* **40** 105211

[95] Guerra-Garcia C and Pavan C A 2023 The Backward Problem in Plasma-Assisted Combustion: Experiments of Nanosecond Pulsed Discharges Driven by Flames *Applications in Energy and Combustion Science* **15** 100155

[96] Palies P, Durox D, Schuller T and Candel S 2010 The Combined Dynamics of Swirler and Turbulent Premixed Swirling Flames *Combust. Flame* **157** 1698–1717

[97] Uhm H S, Choi E H and Cho G 2000 Breakdown Properties of High-Pressure Electrical Discharge *Physics of Plasmas* **7** 2744–2746

[98] Pennell D A, Bothien M R, Ciani A, Granet V, Singla G, Thorpe S, Wickstroem A, Oumejjoud K and Yaquinto M 2017 An Introduction to the Ansaldo GT36 Constant Pressure Sequential Combustor *ASME Turbo Expo 2017: Turbomachinery Technical Conference and Exposition* (American Society of Mechanical Engineers Digital Collection)

[99] Ciani A, Bothien M R, Bunkute B, Wood J P and Früchtel G 2019 Superior Fuel and Operational Flexibility of Sequential Combustion in Ansaldo Energia Gas Turbines *J. Glob. Power Propuls. Soc.* **3** 630–638

[100] Shcherbanev S A, Malé Q, Dharmaputra B, Solana-Pérez R and Noiray N 2022 Effect of Plasma-Flow Coupling on the Ignition Enhancement with Non-Equilibrium Plasma in a Sequential Combustor *J. Phys. D: Appl. Phys.* **55** 425202

[101] Impagnatiello M, Malé Q and Noiray N 2024 Acoustic Scattering of a Sequential Combustor Controlled with Non-Equilibrium Plasma: A Numerical Study *Proc. Combust. Inst.* **40** 105389

[102] Lefkowitz J K and Ombrello T 2018 Reduction of Flame Development Time in Nanosecond Pulsed High Frequency Discharge Ignition of Flowing Mixtures *Combust. Flame* **193** 471–480

[103] Lefkowitz J K, Hammack S D, Carter C D and Ombrello T M 2021 Elevated OH Production from NPHFD and Its Effect on Ignition *Proc. Combust. Inst.* **38** 6671–6678

[104] Adams S, Miles J, Ombrello T, Brayfield R and Lefkowitz J 2019 The Effect of Inter-Pulse Coupling on Gas Temperature in Nanosecond-Pulsed High-Frequency Discharges *J. Phys. D: Appl. Phys.* **52** 355203

[105] Shen S, Laso I, Rozin N and Lefkowitz J K 2023 On Pulse Energy and Energy Distribution for Ignition of Flowing Mixtures *Proc. Combust. Inst.* **39** 5487–5498

[106] Shen S, Rempe E, Senior-Tybora W and Lefkowitz J K 2024 Destructive Inter-Pulse Coupling in Nanosecond-Pulsed High-Frequency Discharge Ignition: Effect of Hydrodynamic Regimes *Proc. Combust. Inst.* **40** 105445

[107] Miller C J, Prashanth P, Allroggen F, Grobler C, Sabnis J S, Speth R L and Barrett S R H 2022 An Environmental Cost Basis for Regulating Aviation NOx Emissions *Environ. Res. Commun.* **4** 055002

[108] Choe J and Sun W 2018 Blowoff Hysteresis, Flame Morphology and the Effect of Plasma in a Swirling Flow *J. Phys. D: Appl. Phys.* **51** 365201

[109] Xiong Y, Schulz O, Bourquard C, Weilenmann M and Noiray N 2019 Plasma Enhanced Auto-Ignition in a Sequential Combustor *Proc. Combust. Inst.* **37** 5587–5594

[110] Blanchard V P, Roqué F, Scouflaire P, Laux C O and Ducruix S 2023 Lean Flames Stabilization With Nanosecond Plasma Discharges in a Gas Turbine Model Combustor *J. Eng. Gas Turbines Power* **146**

[111] Zhang M, Wei X, An Z, Okafor E C, Guiberti T F, Wang J and Huang Z 2025 Flame Stabilization and Emission Characteristics of Ammonia Combustion in Lab-Scale Gas Turbine Combustors: Recent Progress and Prospects *Progress in Energy and Combustion Science* **106** 101193

[112] Tang Y, Xie D, Shi B, Wang N and Li S 2022 Flammability Enhancement of Swirling Ammonia/Air Combustion Using AC Powered Gliding Arc Discharges *Fuel* **313** 122674

[113] Kim G T, Park J, Chung S H and Yoo C S 2022 Effects of Non-Thermal Plasma on Turbulent Premixed Flames of Ammonia/Air in a Swirl Combustor *Fuel* **323** 124227

[114] Zel'dovich Y B 1940 On the Theory of the Propagation of Detonation in Gaseous Systems *Zh. eksp. teoret. fiz.* **10** 542–568

[115] Shkurenkov I, Burnette D, Lempert W R and Adamovich I V 2014 Kinetics of Excited States and Radicals in a Nanosecond Pulse Discharge and Afterglow in Nitrogen and Air *Plasma Sources Sci. Technol.* **23** 065003

[116] Burnette D, Montello A, Adamovich I V and Lempert W R 2014 Nitric Oxide Kinetics in the Afterglow of a Diffuse Plasma Filament *Plasma Sources Sci. Technol.* **23** 045007

[117] Miller J A, Pilling M J and Troe J 2005 Unravelling Combustion Mechanisms through a Quantitative Understanding of Elementary Reactions *Proc. Combust. Inst.* **30** 43–88

[118] Shah Z A, Mehdi G, Congedo P M, Mazzeo D and De Giorgi M G 2024 A Review of Recent Studies and Emerging Trends in Plasma-Assisted Combustion of Ammonia as an Effective Hydrogen Carrier *International Journal of Hydrogen Energy* **51** 354–374

[119] Mao X, Zhong H, Liu N, Wang Z and Ju Y 2024 Ignition Enhancement and NOx Formation of NH3/Air Mixtures by Non-Equilibrium Plasma Discharge *Combustion and Flame* **259** 113140

[120] McDaniel J, Goyne C, Edwards J, Chelliah H, Cutler A and Givi P 2009 US National Center for Hypersonic Combined Cycle Propulsion: An Overview *16th AIAA DLR DGLR International Space Planes and Hypersonic Systems and Technologies Conference* 2009-7280

[121] Vincent-Randonnier A, Mallart-Martinez N and Labaune J 2024 Design of a Plasma-Assisted Injector: Principle, Characterization and Application to Supersonic Combustion of Hydrogen *International Journal of Hydrogen Energy* **88** 1410–1421

[122] Vincent-Randonnier A, Leonov S B and Packan D 2017 First Experiments on Plasma Assisted Supersonic Combustion at LAERTE Facility *55th AIAA Aerosp. Sci. Meet.* (AIAA) 2017-1975

[123] Leonov S B 2018 Electrically Driven Supersonic Combustion *Energies* **11** 1733

[124] Cai Z, Wang T and Sun M 2019 Review of Cavity Ignition in Supersonic Flows *Acta Astronautica* **165** 268–286

[125] Lv C, Chang J, Bao W and Yu D 2022 Recent Research Progress on Air-breathing Aero-Engine Control Algorithm *Propulsion and Power Research* **11** 1–57

[126] Do H, Mungal M G and Cappelli M A 2008 Jet Flame Ignition in a Supersonic Crossflow Using a Pulsed Nonequilibrium Plasma Discharge *IEEE Trans. Plasma Sci.* **36** 2918–2923

[127] Houpt A, Hedlund B, Leonov S, Ombrello T and Carter C 2017 Quasi-DC Electrical Discharge Characterization in a Supersonic Flow *Exp Fluids* **58** 1–17

[128] Leonov B, Hedlund B E and Houpt A W 2018 Morphology of a Q-DC Discharge within a Fuel Injection Jet in a Supersonic Cross-Flow *2018 AIAA Aerosp. Sci. Meet.* (AIAA) 2018-1060

[129] Leonov S, Adamovich I and Soloviev V R 2016 Dynamics of Near-Surface Electric Discharges and Mechanisms of Their Interaction with the Airflow (Topical Review) *Plasma Sources Sci. Technol.* **25** 063001

[130] Braun E L, Hammack S D, Ombrello T M, Lax P and Leonov S B 2024 Enhancement of Chemical Heat Release in a Generic Scramjet Combustor Using Plasma Injection Modules *Proceedings of the Combustion Institute* **40** 105664

[131] Feng R, Huang Y, Zhu J, Wang Z, Sun M, Wang H and Cai Z 2021 Ignition and Combustion Enhancement in a Cavity-Based Supersonic Combustor by a Multi-Channel Gliding Arc Plasma *Experimental Thermal and Fluid Science* **120** 110248

[132] Feng R, Zhu J, Wang Z, Zhang F, Ban Ya, Zhao G, Tian Y, Wang C, Wang H, Cai Z and Sun M 2022 Suppression of Combustion Mode Transitions in a Hydrogen-Fueled Scramjet Combustor by a Multi-Channel Gliding Arc Plasma *Combustion and Flame* **237** 111843

[133] Rocamora A, Tholin F, Bourlet A, Labaune J and Laux C O 2024 Simulation of DC Gliding Arcs for Supersonic Combustion: Influence on O_2/H_2 Ignition *HiSST 2024* (Busan, South Korea)

[134] Ombrello T M, Hammack S D, Carter C D, Busby K and Lefkowitz J K 2024 Scramjet Cavity Ignition Using Nanosecond-Pulsed High-Frequency Discharges *Combust. Flame* **262** 113335

[135] Bourlet A, Tholin F, Labaune J, Pechereau F, Vincent-Randonnier A and Laux C O 2024 Numerical Model of Restrikes in Gliding Arc Discharges *Plasma Sources Sci. Technol.* **33** 015010

[136] Hoffmann H 1940 Reaction-Propulsion Produced by Intermittent Detonative Combustion *Ger. Res. Inst. Glid. Rep. ATI-52365* 161–167

[137] Goto K, Matsuoka K, Matsuyama K, Kawasaki A, Watanabe H, Itouyama N, Ishihara K, Buyakofu V, Noda T and Kasahara J 2023 Space Flight Demonstration of Rotating Detonation Engine Using Sounding Rocket S-520-31 *J. Spacecr. Rockets* **60** 273–285

[138] Ma F, Choi J Y and Yang V 2006 Propulsive Performance of Airbreathing Pulse Detonation Engines *J. Propuls. Power* **22** 1188–1203

[139] Schwer D and Kailasanath K 2011 Numerical Investigation of the Physics of Rotating-Detonation-Engines *Proc. Combust. Inst.* **33** 2195–2202

[140] Wolański P 2013 Detonative Propulsion *Proc. Combust. Inst.* **34** 125–158

[141] Benedick W B, Guirao C M, Knystautas R and Lee J H 1985 Critical Charge for the Direct Initiation of Detonation in Gaseous Fuel-Air Mixtures Tech. Rep. SAND-85-1716C; CONF-850830-6 Sandia National Labs.

[142] Schultz E, Wintenberger E and Shepherd J 1999 Investigation of Deflagration to Detonation Transition for Application to Pulse Detonation Engine Ignition Systems *Proc. 16th JANNAF Propuls. Symp.* vol 1 (Chemical Propulsion Information Agency) pp 175–202

[143] Zhukov V, Rakitin A and Starikovskii A 2007 Detonation Initiation by High-Voltage Pulsed Discharges *45th AIAA Aerosp. Sci. Meet. Exhib.* (AIAA) 2007–1029

[144] Starikovskii A Yu 2003 Deflagration-to-Detonation Control by Non-Equilibrium Gas Discharges and Its Applications for Pulsed Detonation Engine *39th AIAA ASME SAE ASEE Jt. Propuls. Conf. Exhib.* vol 2003–4686

[145] Zhukov V P, Rakitin A E and Starikovskii A Yu 2008 Effect of High-Voltage Pulsed Discharges on Deflagration to Detonation Transition *J. Propuls. Power* **24** 88–93

[146] Rakitin A E and Starikovskii A Yu 2008 Mechanisms of Deflagration-to-Detonation Transition under Initiation by High-Voltage Nanosecond Discharges *Combust. Flame* **155** 343–355

[147] Starikovskii A Yu, Anikin N B, Kosarev I N, Mintoussov E I, Nudnova M M, Rakitin A E, Roupassov D V, Starikovskaia S M and Zhukov V P 2008 Nanosecond-Pulsed Discharges for Plasma-Assisted Combustion and Aerodynamics *J. Propuls. Power* **24** 1182–1197

[148] Rakitin A E and Starikovskii A Yu 2012 Gradient Mechanism of Detonation Initiation under Action of High-Voltage Nanosecond Discharge *J. Propuls. Power* **28** 140–145

[149] Starikovskiy A, Aleksandrov N and A R 2012 Plasma-Assisted Ignition and Deflagration-to-Detonation Transition *Philos. T. R. Soc. A* 740–773

[150] Zel'dovich Y B 1980 Regime Classification of an Exothermic Reaction with Nonuniform Initial Conditions *Combust. Flame* **39** 211–214

[151] Lieberman D, Shepherd J, Wang F and Gundersen M 2005 Characterization of a Corona Discharge Initiator Using Detonation Tube Impulse Measurements *43rd AIAA Aerosp. Sci. Meet. Exhib.* (AIAA) 2005-1344

[152] Wang F, Jiang C, Kuthi A, Gundersen M, Sinibaldi J, Brophy C and Lee L 2004 Transient Plasma Ignition of Hydrocarbon-Air Mixtures in Pulse Detonation Engines *42nd AIAA Aerosp. Sci. Meet. Exhib.* (AIAA) 2004–834

[153] Sinibaldi J, Rodriguez J, Channel B, Brophy C, Wang F, Cathey C and Gundersen M 2005 Investigation of Transient Plasma Ignition for Pulse Detonation Engines *41st AIAA ASME SAE ASEE Jt. Propuls. Conf. Exhib.* (AIAA) 2005–3774

[154] Hutchenson P, Brophy C, Sinibaldi J, Cathey C and Gundersen M 2006 Investigation of Flow Field Properties on Detonation Initiation *42nd AIAA ASME SAE ASEE Jt. Propuls. Conf. Exhib.* (AIAA) 2006–5099

[155] Busby K, Corrigan J, Yu S T, Williams S, Carter C, Schauer F, Hoke J, Cathey C and Gundersen M 2007 Effects of Corona, Spark and Surface Discharges on Ignition Delay and Deflagration-to-Detonation Times in Pulsed Detonation Engines *45th AIAA Aerosp. Sci. Meet. Exhib.* (AIAA) 2007–1028

[156] Cathey C, Wang F, Tang T, Kuthi A, Gundersen M, Sinibaldi J, Brophy C, Barbour E, Hanson R and Hoke J 2007 Transient Plasma Ignition for Delay Reduction in Pulse Detonation Engines *45th AIAA Aerosp. Sci. Meet. Exhib.* (AIAA) 007–443

[157] Singleton D, Pendleton S J and Gundersen M A 2010 The Role of Non-Thermal Transient Plasma for Enhanced Flame Ignition in C2H4–Air *J. Phys. Appl. Phys.* **44** 022001

[158] Singleton D R, Sinibaldi J O, Brophy C M, Kuthi A and Gundersen M A 2009 Compact Pulsed-Power System for Transient Plasma Ignition *IEEE Trans. Plasma Sci.* **37** 2275–2279

[159] Singleton D, Gundersen M A and Simone A 2010 Optimization of Compact Power Modulators for Transient Plasma Ignition *2010 IEEE Int. Power Modul. High Volt. Conf.* pp 254–257

[160] Zheng D 2016 The Advantages of Non-Thermal Plasma for Detonation Initiation Compared with Spark Plug *Plasma Sci. Technol.* **18** 162

[161] Zheng D and Wang B 2018 Acceleration of DDT by Non-Thermal Plasma in a Single-Trial Detonation Tube *Chin. J. Aeronaut.* **31** 1012–1019

[162] Zheng D F and Wang B 2018 Utilization of Nonthermal Plasma in Pulse Detonation Engine Ignition *J. Propuls. Power* **34** 539–549

[163] Gray J A and Lacoste D A 2019 Enhancement of the Transition to Detonation of a Turbulent Hydrogen–Air Flame by Nanosecond Repetitively Pulsed Plasma Discharges *Combust. Flame* **199** 258–266

[164] Gray J A and Lacoste D A 2019 Effects of Nanosecond Repetitively Pulsed Plasma Discharges on a Propagating Hydrogen–Air Flame (American Institute of Aeronautics and Astronautics, AIAA)

[165] Gray J A T and Lacoste D A 2021 Effect of the Plasma Location on the Deflagration-to-Detonation Transition of a Hydrogen-Air Flame Enhanced by Nanosecond Repetitively Pulsed Discharges *Proc. Combust. Inst.* **38** 3463–3472

[166] Vorenkamp M, Steinmetz S A, Chen T Y, Mao X, Starikovskiy A Yu, Kliewer C and Ju Y 2023 Plasma-Assisted Deflagration to Detonation Transition in a Microchannel with Fast-Frame Imaging and Hybrid Fs/Ps Coherent Anti-Stokes Raman Scattering Measurements *Proc. Combust. Inst.* **39** 5561–5569

[167] Vorenkamp M, Steinmetz S, Mao X, Shi Z, Starikovskiy A Yu, Ju Y and Kliewer C 2023 Effect of Plasma-Enhanced Low-Temperature Chemistry on Deflagration-to-Detonation Transition in a Microchannel *AIAA J.* **61** 4821–4827

[168] Shi Z, Mao X and Ju Y 2023 Numerical Modeling of Plasma Assisted Deflagration to Detonation Transition of a H_2/O_2 Mixture in a Microscale Channel *AIAA Scitech 2023 Forum* vol 2023–0346

[169] Shi Z, Mao X, Thawko A and Ju Y 2024 Numerical Modeling of Plasma Assisted Deflagration to Detonation Transition in a Microscale Channel *Proc. Combust. Inst.* **40** 105659

[170] Thawko A, Vorenkamp M, Shi Z, Mao X and Ju Y 2024 The Effect of Ozone Kinetic Enhancement on Detonation Transition in a Microchannel with Dimethyl Ether Mixture *AIAA Scitech 2024 Forum* (AIAA) 2024–0405

[171] Thawko A, Cao Y, Shi Z, Vorenkamp M, Wang Z, Mei B, Mao X and Ju Y 2024 Accelerated Ignition-Shock Coupling and Deflagration to Detonation Transition by Ozone Kinetic Enhancement of Dimethyl Ether Mixture *Proc. Combust. Inst.* **40** 105517

[172] Lafaurie V, Shu Z, Vidal P and Starikovskaia S M 2024 Gradient Pulsed Transient Plasma for Initiation of Detonation *Combust. Flame* **261** 113311

[173] Lafaurie V 2025 *Pulsed Plasma Approach for Mild or Strong Ignition of a Detonation Wave Using a Gradient of Atomic Species.* Ph.D. thesis Ecole Polytechnique

[174] Zhou S, Wang F, Che X and Nie W 2016 Numerical Study of Nonequilibrium Plasma Assisted Detonation Initiation in Detonation Tube *Phys. Plasmas* **23** 123522

[175] Zhou S, Nie W, Che X, Chen Q and Zhang Z 2017 Influence of Equivalence Ratio on Plasma Assisted Detonation Initiation by Alternating Current Dielectric Barrier Discharge under Rich Burn Condition *Aerosp. Sci. Technol.* **69** 504–512

[176] Tropina A A, Mahamud R, Yorn D W and Miles R B 2019 Deflagration to Detonation Transition Assisted by Equilibrium and Non-Equilibrium Plasma *AIAA Aviat. 2019 Forum* (AIAA) 2019–3119

[177] Tropina A A and Mahamud R 2022 Effect of Plasma on the Deflagration to Detonation Transition *Combust. Sci. Technol.* **194** 2752–2770

[178] AliCherif M, Masuda R, Claverie A, Starikovskaia S and Vidal P 2024 Plasma-Enhanced Detonability: Experimental and Calculated Reduction of the Detonation Cell Size *Combust. Flame* **268** 113639

[179] Cherif M A, Shcherbanev S A, Starikovskaia S M and Vidal P 2020 Effect of Non-Equilibrium Plasma on Decreasing the Detonation Cell Size *Combust. Flame* **217** 1–3

[180] Zhu Y, Anand V, Jodele J, Knight E, Gutmark E J and Burnette D 2017 Plasma-Assisted Rotating Detonation Combustor Operation *53rd AIAA SAE ASEE Jt. Propuls. Conf.* (AIAA) 2017–4742

[181] Nijdam S, Teunissen J and Ebert U 2020 The Physics of Streamer Discharge Phenomena *Plasma Sources Sci. Technol.* **29** 103001

[182] Pai D Z, Lacoste D A and Laux C O 2010 Transitions between Corona, Glow, and Spark Regimes of Nanosecond Repetitively Pulsed Discharges in Air at Atmospheric Pressure *Journal of Applied Physics* **107** 093303

[183] Maly R R and Herweg R 2008 Spark Ignition and Combustion in Four-Stroke Gasoline Engines *Flow and Combustion in Reciprocating Engines* (Springer, Berlin, Heidelberg) pp 1–66 ISBN 978-3-540-68901-0

[184] van der Horst R M, Verreycken T, van Veldhuizen E M and Bruggeman P J 2012 Time-Resolved Optical Emission Spectroscopy of Nanosecond Pulsed Discharges in Atmospheric-Pressure N2 and N2/H2O Mixtures *J. Phys. D: Appl. Phys.* **45** 345201

[185] Stepanyan S A, Starikovskiy A Yu, Popov N A and Starikovskaia S M 2014 A Nanosecond Surface Dielectric Barrier Discharge in Air at High Pressures and Different Polarities of Applied Pulses: Transition to Filamentary Mode *Plasma Sources Sci. Technol.* **23** 045003

[186] Shcherbanev S A, Yu Khomenko A, Stepanyan S A, Popov N A and Starikovskaia S M 2016 Optical Emission Spectrum of Filamentary Nanosecond Surface Dielectric Barrier Discharge *Plasma Sources Sci. Technol.* **26** 02LT01

[187] Lo A, Cessou A, Lacour C, Lecordier B, Boubert P, Xu D A, Laux C O and Vervisch P 2017 Streamer-to-Spark Transition Initiated by a Nanosecond Overvoltage Pulsed Discharge in Air *Plasma Sources Sci. Technol.* **26** 045012

[188] Orrière T, Moreau E and Pai D Z 2018 Ionization and Recombination in Nanosecond Repetitively Pulsed Microplasmas in Air at Atmospheric Pressure *J. Phys. D: Appl. Phys.* **51** 494002

[189] Shcherbanev S A, Ding Ch, Starikovskaia S M and Popov N A 2019 Filamentary Nanosecond Surface Dielectric Barrier Discharge. Plasma Properties in the Filaments *Plasma Sources Sci. Technol.* **28** 065013

[190] Sainct F P, Urabe K, Pannier E, Lacoste D A and Laux C O 2020 Electron Number Density Measurements in Nanosecond Repetitively Pulsed Discharges in Water Vapor at Atmospheric Pressure *Plasma Sources Sci. Technol.* **29** 025017

[191] Minesi N, Stepanyan S, Mariotto P, Stancu G D and Laux C O 2020 Fully Ionized Nanosecond Discharges in Air: The Thermal Spark *Plasma Sources Sci. Technol.* **29** 085003

[192] Minesi N Q, Mariotto P B, Pannier E, Vincent-Randonnier A, Stancu G D and Laux C O 2023 Kinetic Mechanism and Sub-Ns Measurements of the Thermal Spark in Air *Plasma Sources Sci. Technol.* **32** 044005

[193] Zhang B, Zhu Y, Zhang X, Popov N, Orriere T, Pai D Z and Starikovskaia S M 2023 Streamer-to-Filament Transition in Pulsed Nanosecond Atmospheric Pressure Discharge: 2D Numerical Modeling *Plasma Sources Sci. Technol.* **32** 115014

[194] Maillard J, Pannier E and Laux C O 2025 CO2 Conversion by NRP Discharges: Spotlight on Two Parallel CO Production Mechanisms, *Plasma Sources Sci. Technol.* In submission

[195] Roger E, Mariotto P and Laux C O 2025 Origin of the Recirculation Flow Pattern Induced by Nanosecond Discharges and Criterion for Its Development *J. Phys. D: Appl. Phys.* **58** 145203